

Chapter V

BAY OF BENGAL: PALAEOCLIMATIC IMPLICATIONS

Sedimentation in the Bay of Bengal is governed primarily by detrital input through various rivers draining into it and by overhead primary productivity. The composition of the sediments brought in by the various river systems depends on the terrain through which they flow (Sarin et al., 1989; Somayajulu et al., 1993, 2002). Erosion, composition, transportation and deposition processes of terrigenous sediments into the Bay of Bengal are essentially controlled by crustal deformation (tectonic) and climatic conditions (effect of monsoon). In the open oceans, these sediments serve as an archive of the Earth's geological history where effects of tectonics, climatic changes and eustasy are recorded and preserved. Rivers originating from the Himalayan regions contribute ~20% of the global sediment input to the Bay of Bengal (Milliman and Meade, 1983). The Ganga along with the Brahmaputra (the G-B River system) is one of the major contributors of sediment to the global ocean, transporting about 729×10^6 tons of sediment load annually to the Bay of Bengal (Coleman, 1969; Milliman and Syvitski, 1992; Curray, 1994). Nearly one third of the sediments discharged by the G-B River system is deposited in the shelf areas (Kuehl et al., 1997). As a result, the G-B River system has the largest delta and the largest submarine deep sea fan.

Sediment transfer from the continental areas to the Bay of Bengal is mainly governed by two distinct fluvial regimes, namely the Himalayan and the Peninsular Rivers. The G-B River system is the major contributor, however, in the Andaman Sea on the eastern Bay of Bengal, an additional contribution comes from the Irrawaddy and Salween Rivers (Rodolfo, 1969;

Sarin et al., 1979; Rao and Kessarkar, 2001; Rao et al., 2005; Chauhan et al., 2005). Besides this, the Bay of Bengal experiences a steady rain of biogenic debris which also contributes to the sedimentary budget. Considering that the sediment flux is intimately associated with the tectonic and

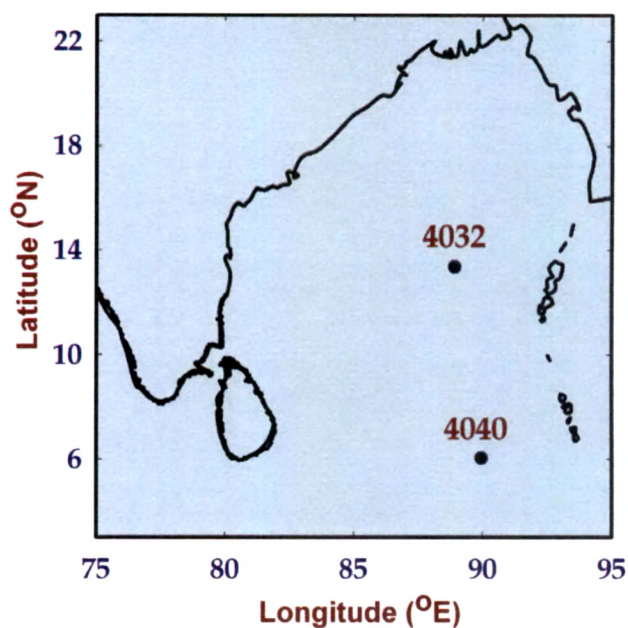


Fig. 5.1: Sediment core locations in the Bay of Bengal

climatic variability (monsoon), the sedimentary archive in the Bay of Bengal provides a rare opportunity to reconstruct the past climatic (Gupta and Thomas, 2003) and tectonic activity (Metivier and Gaudemer, 1999). It has been suggested that the monsoon driven hydrological changes caused significant variability in geochemical and isotopic proxies (Kudrass et al., 2001), so much so that centennial to millennial scale changes can be ascertained by careful investigation of sediment cores (Colin et al., 1998).

In the present study, signatures of geochemical and isotopic composition, total organic carbon (TOC) and carbon/nitrogen (C/N) ratio of the sediments have been used to reconstruct Late Quaternary climatic changes from two gravity cores viz. 4032 and 4040 collected from the central and southern Bay of Bengal respectively (Fig. 5.1). Considering that the detrital contribution is regulated through distinct fluvial systems, this study also attempts to investigate temporal change in contribution from different sources (provenance) during the sedimentation process to study the past erosional patterns. The central Bay of Bengal core 4032 (13.36°N; 88.9°E) was 148 cm in length raised from 3011 m water depth. The sediments in the core are

sandy and light coloured, foraminiferal ooze. However, the southern Bay of Bengal core 4040 (6.03°N; 89.94°E) was raised from relatively shallower water depth (2788 m) and was located at top of the 90° East Ridge (Fig. 5.1). The length of the core 4040 was 140 cm, contained whitish foram rich ooze. The core location 4032 represents a region of high detrital flux and overhead productivity in the central Bay of Bengal, whereas core 4040 (southern Bay of Bengal) has low detrital flux and moderate overhead productivity (Ramaswamy and Nair, 1994). Reconstruction of spatial and temporal changes in Late Quaternary climate and provenance was attempted using the geochemical, lithogenic and isotopic proxies, which were then viewed with respect to regional and global climatic pattern (Naidu and Malmgren, 1996, 1999; Naidu, 2007).

Chronology and Sedimentation Rates

Chronology, which constitutes the major component in any palaeoclimatic study, was obtained using the Accelerated Mass Spectrometry

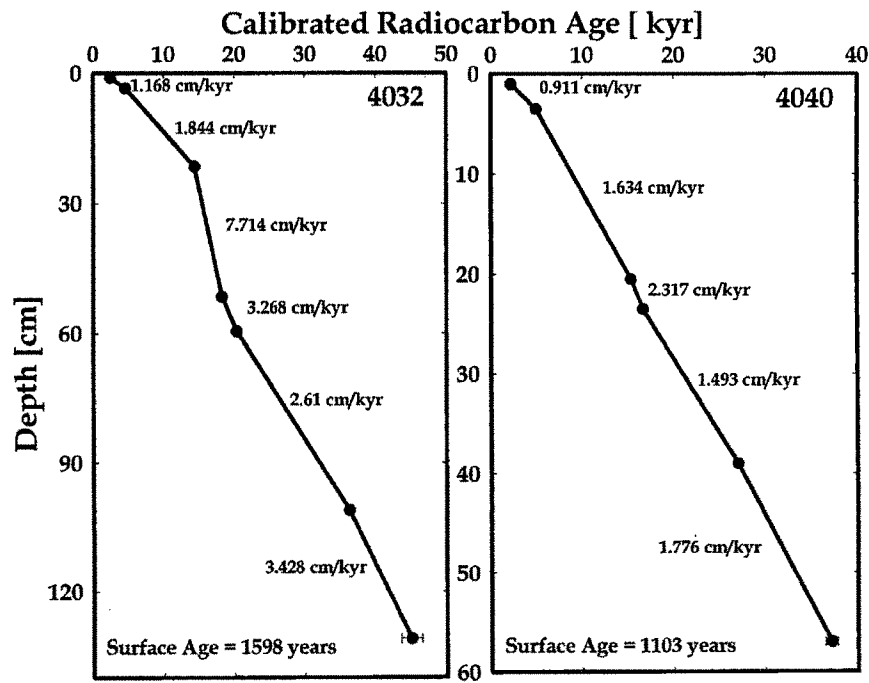


Fig. 5.2: Age-Depth plot model of the core 4032 and 4040 from the Bay of Bengal.

(AMS) radiocarbon dating of surface dwelling planktonic foraminifer (viz. *Globigerina Ruber*, *Globigerina Sacculifer* etc). Samples for AMS radiocarbon dating were collected from selected depths (Fig. 5.2) and a suite of planktonic foraminifer was separated by wet sieving. The AMS radiocarbon dating was carried out at National Science Foundation–Accelerated Mass Spectrometry (AMS) Facility at the University of Arizona, Tucson (USA). In case of core 4040, only the upper 60 cm was considered because it was a double bounce core beyond 80 cm. Ages thus obtained were calibrated

**Table 5.1: AMS ¹⁴C dates of foraminifer shells from the Cores 4032 and 4040
Core: 4040**

Depth (cm)	AMS ¹⁴ C Age (yrs)	Error on ¹⁴ C Age	Calibrated ¹⁴ C Age (yrs BP)	Errors on Calibrated Age
0-2	2550	38	2201	67
3-4	4757	49	4946	80
20-21	13437	98	15348	183
23-24	14401	93	16643	223
38-40	23080	180	27028	211
56-58	31990	570	37165	662

Core: 4032

Depth (cm)	AMS ¹⁴ C Age (yrs)	Error on ¹⁴ C Age	Calibrated ¹⁴ C Age (yrs)	Error on Calibrated Age (yrs BP)
0-2	2788	45	2454	96
3-4	4455	46	4595	88
21-22	12958	85	14358	242
51-52	15445	87	18247	135
59-60	17660	110	20337	143
100-102	31140	510	36240	594
130-132	39700	1300	44992	1489

to calendar years using CALIB 4.1 (Stuiver et al., 1998a) with a ΔR value correction of 22 yrs (Dutta et al., 2001). A total of seven samples from core 4032 were dated and the ages range from 44992 ± 1489 (at 130–132 cm) to 2454 ± 96 cal yr (at 0–2 cm). In case of core 4040, six samples were analyzed and the ages range from 37165 ± 662 cal yr to 2201 ± 67 cal yr (Table-5.1). The extrapolated surface age for the core 4032 was 1598 years whereas for core 4040 it was 1103 years (Table 5.1, Fig. 5.2). The ages enabled to develop an age–depth model and the ages of intermediate depths were obtained by interpolation. However, sedimentation rate was calculated between actual adjacent ages (Fig. 5.2).

A significant variability in the sedimentation rate was observed in core 4032 which ranges from 7.714 cm/kyr (between 18247 cal yr to 14358 cal yr) and 1.168 cm/kyr (between 4595 cal yr to 2454 cal yr, Fig. 5.2). Compared to this, core 4040 shows marginal variability in sedimentation rate ranging from 2.317 cm/kyr (between 16643 cal yr to 15348 cal yr) and 0.911 cm/kyr (between 4946 cal yr to 2201 cal yr, Fig. 5.1). In addition, Mass Accumulation Rate (MAR) was calculated ($\text{g}/\text{cm}^2/\text{kyr}$) in the core 4032 to determine the sediment flux of the various elements. It was observed that between 50 kyr to ~21 kyr, the MAR fluctuated around $4 \text{ g}/\text{cm}^2/\text{kyr}$, except around 40 kyr when it marginally increased ($\sim 5 \text{ g}/\text{cm}^2/\text{kyr}$). However, after 20 kyr and 14 kyr, a significant increase of $\sim 13 \text{ g}/\text{cm}^2/\text{kyr}$ was observed.

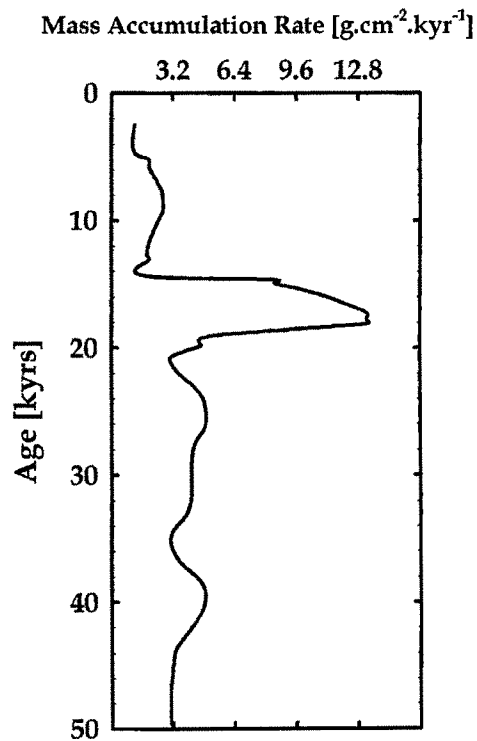


Fig. 5.3: Mass Accumulation Rate for the core 4032.

Following this, a consistent low MAR centering around $2 \text{ g.cm}^{-2}.\text{kyr}^{-1}$ persisted till around 2.5 kyr (Fig. 5.3).

Variation in Lithogenic Proxies

Sediment trap studies in the central Bay of Bengal show that the lithogenic flux is around $32 \text{ g.m}^{-2}.\text{day}^{-1}$ in shallow trap (995 m), and it

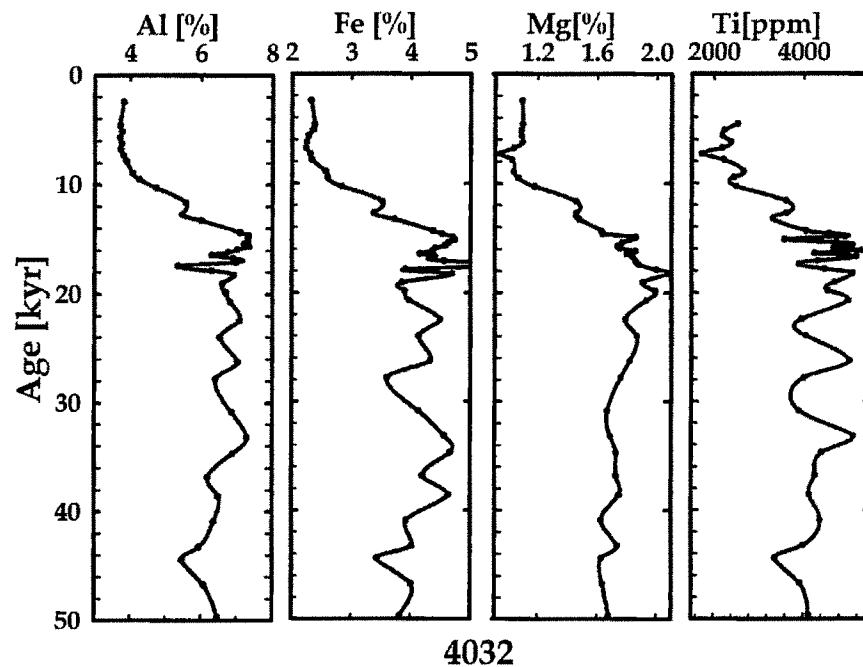


Fig. 5.4: Downcore variation of Al (%), Fe(%), Mg(%) and Ti(ppm) in the core 4032. In general, a slow decreasing pattern from 50 kyr to 14 kyr and a gradual decreasing pattern from 14 kyr to 7 kyr can be noticed.

almost doubled at $64 \text{ g.m}^{-2}.\text{day}^{-1}$ in the deep trap (2291 m) in the central Bay of Bengal during August, whereas during April–May, it increased marginally from $12 \text{ g.m}^{-2}.\text{day}^{-1}$ in shallow trap to $16 \text{ g.m}^{-2}.\text{day}^{-1}$ in the deep trap (Ramaswamy et al., 1997). Studies have shown that the lithogenic and the biogenic fluxes in the Bay of Bengal show identical patterns particularly during the southwest monsoon, which is attributed to the increased suspended load and increase in primary productivity facilitating efficient scavenging of the lithogenic particles (Ramaswamy et al., 1997). The

scavenging of the lithogenic particles is high during SW monsoon period due to a simultaneous increase in primary productivity and suspended load of the Bay of Bengal. Compared to this, discordance in lithogenic and biogenic flux was observed during winter monsoon, which is attributed to the reduction in fluvial discharge leading to the reduced lithogenic flux (Ramaswamy and Nair, 1994).

The concentration of the major elements as Al, Fe, Mg and Ti is used as a proxy for the continental terrigenous input to the oceans (Table 5.2; Goldberg and Arrhenius, 1958; Lisitsyn, 1972; Taylor and McLennan, 1985; Measures et al., 1986; Agnihotri et al., 2003). For example, Al belongs to the hydrolyzate elements and is not drawn into the biological cycle. Thus, its distribution in marine sediments reflects a terrigenous and volcanogenic source and is the second most widely distributed element (average concentration ~ 15%) in sedimentary deposits after silica (Lisitsyn, 1996; Dymond et al., 1997). Nature of distribution of Fe in ocean sediment is due to its participation in the biological cycle. In spite of this, Fe is associated both with sandy (proximal to ocean margins) and clayey fractions in pelagic realm (Skornyakova, 1970). In the equatorial zone, increased accumulation of Fe is observed in association with the fine grained sediments in coastal regions of Atlantic and Indian Oceans (Bostrom et al., 1973; Lisitsyn, 1996). The high concentration of Mg in marine sediments is associated with the basaltic rocks and thus its concentration can be used to identify the regions dominated by basaltic lithology. Additionally, it can also be contributed from the oceanic crust, and in few cases as terrigenous aeolian input (e.g. the Arabian Sea and the Indian Ocean; Lisitsyn, 1996). Ti and Fe are closely associated due to their identical ionic radii; however the latter is chemically stable, indicated by identical pattern of distribution (no grain size preference) in fluvial sediments (Lisitsyn, 1996).

The down core concentration variation of major elements (Al, Fe, Mg and Ti) in central Bay of Bengal (core-4032) shows a (i) consistent high values and low frequency fluctuations between 50 kyr and 14 kyr with an abrupt

Table: 5.2: Concentrations of Major and Trace elements in the bulk sediments of the core 4032

Core	Depth (cm)	Age (yrs)	Sr (ppm)	Cr (ppm)	Ba (ppm)	Mn (%)	Fe (%)	Mg (%)	Al (%)	Ca (%)
4032[0-2]	1	2454	726	44	729	0.16	2.3	1.10	3.8	23.4
4032[3-4]	3.5	4595	759	53	816	0.17	2.4	1.10	3.7	19.5
4032[4-5]	4.5	5137	745	57	865	0.19	2.4	1.09	3.8	19.5
4032[5-6]	5.5	5680	727	54	830	0.14	2.3	1.09	3.7	19.2
4032[6-7]	6.5	6222	735	56	854	0.18	2.3	1.10	3.8	18.7
4032[7-8]	7.5	6765	762	61	843	0.20	2.2	1.04	3.7	20.0
4032[8-9]	8.5	7307	715	60	649	0.22	2.3	0.95	3.8	20.2
4032[9-10]	9.5	7849	670	57	790	0.25	2.3	1.03	3.9	19.1
4032[11-12]	11.5	8934	646	67	706	0.37	2.6	1.04	4.1	17.6
4032[12-13]	12.5	9476	615	61	798	0.35	2.6	1.07	4.3	17.2
4032[13-15]	14	10290	538	59	707	0.40	2.8	1.18	4.7	16.0
4032[16-17]	16.5	11646	394	76	588	1.53	3.5	1.46	5.6	10.1
4032[18-19]	18.5	12731	448	77	695	2.31	3.4	1.46	5.5	12.0
4032[19-20]	19.5	13273	388	79	623	1.09	3.7	1.48	6.0	10.8
4032[21-22]	21.5	14358	277	91	487	0.49	4.4	1.63	7.1	6.8
4032[23-24]	23.5	14617	195	96	435	0.72	4.5	1.64	7.3	3.9
4032[25-26]	25.5	14877	242	99	582	2.23	4.7	1.86	7.3	4.7
4032[27-28]	27.5	15136	235	92	520	1.02	4.7	1.82	7.3	5.5
4032[29-30]	29.5	15395	239	88	511	0.57	4.6	1.77	7.2	5.4
4032[31-32]	31.5	15654	287	107	489	0.09	4.6	1.74	7.4	5.9
4032[33-34]	33.5	15914	286	102	502	0.07	4.4	1.75	7.0	6.4
4032[35-36]	35.5	16173	355	102	620	0.09	4.4	1.86	6.8	7.9
4032[37-38]	37.5	16432	388	94	650	0.10	4.2	1.80	6.3	8.7
4032[39-40]	39.5	16691	342	95	666	0.29	4.4	1.84	6.9	7.4
4032[42-43]	42.5	17080	302	101	553	0.08	4.6	1.86	7.0	7.0
4032[44-46]	45	17404	382	77	546	0.95	6.4	1.88	5.4	7.5
4032[48-49]	48.5	17858	359	92	606	0.08	3.9	2.00	6.3	8.8
4032[51-52]	51.5	18247	272	100	576	0.09	4.7	2.08	6.9	5.9
4032[54-55]	54.5	19031	322	99	535	0.07	3.9	1.91	6.6	7.5
4032[57-58]	57.5	19814	312	96	580	0.09	3.9	1.99	6.7	7.4
4032[60-61]	60.5	20720	313	100	562	0.10	4.0	1.93	6.8	7.6
4032[64-66]	65	22444	209	99	466	0.09	4.5	1.79	7.1	4.7
4032[68-70]	69	23977	309	93	538	0.10	4.1	1.87	6.5	7.5
4032[74-76]	75	26276	259	100	530	0.10	4.3	1.82	6.0	5.9
4032[78-80]	79	27809	373	92	582	0.10	3.6	1.76	6.4	9.3
4032[86-88]	87	30875	336	102	574	0.10	4.1	1.67	6.9	8.3
4032[92-94]	93	33174	265	107	439	0.10	4.6	1.69	7.3	5.8
4032[96-98]	97	34707	263	101	444	0.12	4.7	1.73	6.9	5.8
4032[102-104]	103	36824	356	90	556	0.13	4.2	1.73	6.2	8.8
4032[108-110]	109	38574	294	103	594	0.14	4.6	1.75	6.5	6.1
4032[116-118]	117	40908	366	97	602	0.11	3.9	1.63	6.4	8.8
4032[124-126]	125	43242	434	93	683	0.14	4.0	1.74	6.0	9.6
4032[128-130]	129	44409	497	95	711	0.13	3.4	1.63	5.5	10.9
4032[136-138]	137	46743	465	105	818	0.13	4.0	1.64	6.1	10.0
4032[146-148]	147	49660	397	107	708	0.11	3.8	1.68	6.5	9.0

Table 5.2 contd.

Core	Depth (cm)	Age (yrs)	Ni (ppm)	Co (ppm)	Zn (ppm)	Cu (ppm)	V (ppm)	Ti (ppm)
4032[0-2]	1	2454	--	--	--	--	--	--
4032[3-4]	3.5	4595	140	37	93	99	94	2535
4032[4-5]	4.5	5137	148	36	88	97	89	2245
4032[5-6]	5.5	5680	118	34	90	98	85	2192
4032[6-7]	6.5	6222	133	36	91	103	86	2379
4032[7-8]	7.5	6765	142	33	80	95	83	2183
4032[8-9]	8.5	7307	134	29	74	85	65	1735
4032[9-10]	9.5	7849	137	32	82	97	83	2222
4032[11-12]	11.5	8934	186	38	108	116	106	2666
4032[12-13]	12.5	9476	194	39	114	109	99	2447
4032[13-15]	14	10019	185	34	99	85	105	2503
4032[16-17]	16.5	11646	358	52	200	142	156	3616
4032[18-19]	18.5	12731	286	58	159	123	168	3621
4032[19-20]	19.5	13273	183	32	124	80	141	3322
4032[21-22]	21.5	14358	195	41	129	70	156	4052
4032[23-24]	23.5	14617	276	54	147	77	187	4575
4032[25-26]	25.5	14877	482	83	167	104	183	4924
4032[27-28]	27.5	15136	273	65	140	67	174	3582
4032[29-30]	29.5	15395	226	57	150	83	191	4726
4032[31-32]	31.5	15654	213	45	149	84	191	5066
4032[33-34]	33.5	15914	223	43	162	95	190	4660
4032[35-36]	35.5	16173	198	42	151	81	181	5276
4032[37-38]	37.5	16432	197	38	146	88	168	4247
4032[39-40]	39.5	16691	241	66	151	93	175	5175
4032[42-43]	42.5	17080	220	40	161	93	163	4309
4032[44-46]	45	17405	221	62	146	68	187	3905
4032[48-49]	48.5	17858	217	38	154	84	190	4471
4032[51-52]	51.5	18247	254	47	173	84	185	5086
4032[54-55]	54.5	19031	251	40	178	121	211	4694
4032[57-58]	57.5	19814	262	47	179	103	179	4546
4032[60-61]	60.5	20720	285	49	197	115	195	4994
4032[64-66]	65	22445	208	36	144	62	142	3961
4032[68-70]	69	23978	218	39	164	91	152	4065
4032[74-76]	75	26276	272	49	197	110	203	5024
4032[78-80]	79	27809	258	42	192	133	176	4023
4032[86-88]	87	30875	224	37	155	69	154	3912
4032[92-94]	93	33174	295	49	196	70	191	5104
4032[96-98]	97	34707	255	44	172	68	156	4412
4032[102-104]	103	36824	242	44	160	96	143	4258
4032[108-110]	109	38574	258	47	177	91	150	4134
4032[116-118]	117	40908	254	42	181	91	147	4375
4032[124-126]	125	43242	258	50	180	103	184	3993
4032[128-130]	129	44409	209	35	144	103	131	3376
4032[136-138]	137	46743	260	47	175	87	157	3924
4032[146-148]	147	49660	261	52	175	105	188	4118

decrease around 17 kyr in Al and Ti, (ii) a gradual decrease after 14 kyr which persisted till around 7 kyr and (iii) a consistently low values after 7 kyr till 2 kyr (Fig. 5.4). The association of Al with the lithogenically derived elements can serve as an indicator for Al content in opal which reflects the relative availability of iron and other trace nutrients (Dymond et al., 1997).

In case of the southern Bay of Bengal (core 4040), a high variability in the concentration of geochemical proxies is observed (Table 5.3). The down core variability indicates low frequency high magnitude fluctuations between 36 kyr and 3 kyr. A gradual increase after 36 kyr till 32 kyr followed by an abrupt decrease in Al, Fe and Mg around 30 kyr. This has been succeeded by an overall increase till around 22 kyr followed by a dip in the concentration of the above elements centering around 20 kyr (except for Mg). This was followed by an increase peaking around 14.5 kyr. After 14.5 kyr, a marginal decline in the geochemical proxies is noticed between 12.5 kyr to 10 kyr. After 10 kyr till 3 kyr, an increasing trend can be suggested though Mg and Ti show a decreasing trend (Fig.5.5).

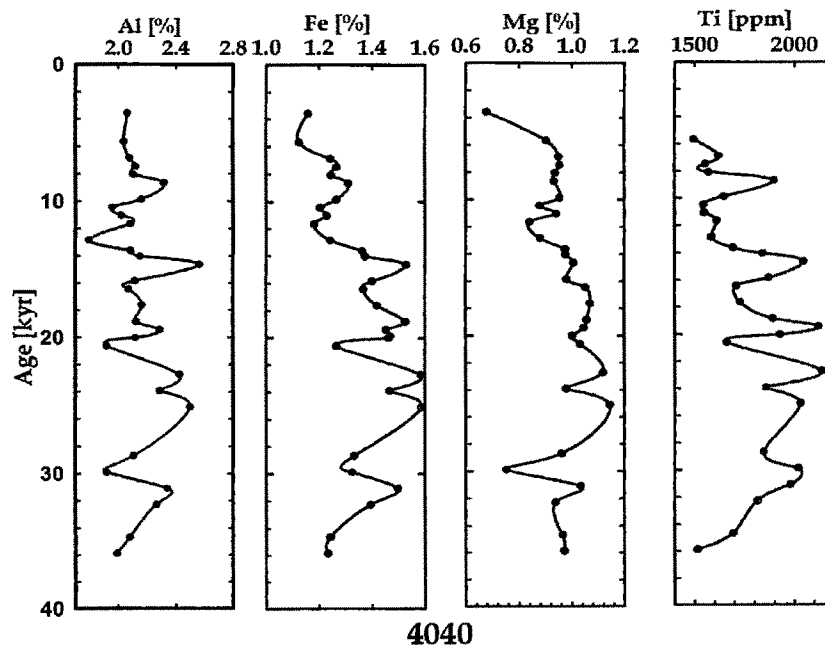


Fig. 5.5: Downcore variation of Al (%), Fe (%), Mg (%) and Ti (ppm) in the core 4040. Note, relatively high variability in their concentrations.

Table: 5.3: Concentrations of Major and Trace elements in the bulk sediments of the core 4040.

Core	Depth (cm)	Age (yrs)	Al (%)	Fe (%)	Mg (%)	Ca (%)	Sr (ppm)	Ba (ppm)	Ni (ppm)
4040[0-2]	1	3579	2.06	1.16	0.68	28.9	923	730	22
4040[4-5]	4.5	5671	2.04	1.12	0.90	16.6	1917	1530	85
4040[6-7]	6.5	6866	2.08	1.24	0.95	16.2	1890	1717	53
4040[7-8]	7.5	7464	2.12	1.27	0.95	16.5	1923	1680	71
4040[8-9]	8.5	8062	2.10	1.24	0.94	15.9	1811	1691	52
4040[9-10]	9.5	8659	2.32	1.31	0.93	15.6	1768	1699	73
4040[11-12]	11.5	9855	2.16	1.27	0.95	16.3	1847	1617	57
4040[12-13]	12.5	10453	1.96	1.20	0.88	15.7	1775	1580	52
4040[13-14]	13.5	11050	2.02	1.23	0.94	15.9	1829	1587	48
4040[14-15]	14.5	11648	2.08	1.18	0.84	15.8	1796	1460	68
4040[16-17]	16.5	12844	1.79	1.24	0.88	15.6	1753	1318	57
4040[17-18]	17.8	13621	2.08	1.36	0.97	15.8	1879	1423	90
4040[18-19]	18.5	14039	2.15	1.37	0.98	15.6	1873	1474	88
4040[19-20]	19.5	14637	2.56	1.53	1.01	16.0	1796	1473	147
4040[21-22]	21.5	15832	2.12	1.40	0.98	15.7	1766	1304	70
4040[22-23]	22.5	16430	2.07	1.37	1.05	15.6	1870	1273	55
4040[24-25]	24.5	17625	2.16	1.42	1.07	15.8	1845	1238	67
4040[26-27]	26.5	18821	2.12	1.52	1.06	15.7	1859	1233	49
4040[27-28]	27.5	19419	2.29	1.45	1.05	15.4	1786	1336	50
4040[28-29]	28.5	20016	2.12	1.46	1.00	14.9	1712	1137	50
4040[29-30]	29.5	20614	1.92	1.27	1.03	15.9	1840	1071	67
4040[32-34]	33	22706	2.42	1.58	1.12	15.5	1898	1225	58
4040[34-36]	35	23902	2.29	1.47	0.98	15.5	1832	1113	51
4040[36-38]	37	25097	2.50	1.59	1.14	15.6	1762	1231	61
4040[42-44]	43	28683	2.10	1.33	0.96	15.4	1872	1135	49
4040[44-46]	45	29879	1.92	1.33	0.75	14.5	1676	1171	51
4040[46-48]	47	31074	2.34	1.50	1.03	15.6	1806	1238	54
4040[48-50]	49	32270	2.26	1.39	0.94	15.8	1784	1291	63
4040[52-54]	53	34661	2.08	1.24	0.97	16.3	1751	1234	55
4040[54-56]	55	35856	1.99	1.23	0.97	16.2	1738	1214	56

Table 5.3 Contd.

Core	Depth (cm)	Age (yrs)	Co (ppm)	Cr (ppm)	Mn (ppm)	Zn (ppm)	Cu (ppm)	V (ppm)	Ti (ppm)
4040[0-2]	1	3579	16	20	648	--	--	--	--
4040[4-5]	4.5	5671	20	63	1369	92	10	55	1495
4040[6-7]	6.5	6866	21	73	1367	64	65	56	1622
4040[7-8]	7.5	7464	23	69	1443	65	64	55	1554
4040[8-9]	8.5	8062	21	70	1471	63	66	58	1571
4040[9-10]	9.5	8659	22	70	1612	88	108	66	1899
4040[11-12]	11.5	9855	20	68	1454	97	108	56	1646
4040[12-13]	12.5	10453	21	67	1703	61	64	53	1547
4040[13-14]	13.5	11050	20	71	1464	59	61	53	1548
4040[14-15]	14.5	11648	22	66	1370	92	88	55	1611
4040[16-17]	16.5	12844	21	70	1350	65	63	54	1585
4040[17-18]	17.8	13621	26	69	1901	68	64	62	1694
4040[18-19]	18.5	14039	26	73	2547	73	71	63	1841
4040[19-20]	19.5	14637	33	80	3848	115	113	74	2046
4040[21-22]	21.5	15832	60	74	2179	71	60	67	1872
4040[22-23]	22.5	16430	55	76	1408	69	54	62	1710
4040[24-25]	24.5	17625	62	86	1159	94	107	63	1729
4040[26-27]	26.5	18821	30	85	617	74	54	67	1893
4040[27-28]	27.5	19419	24	85	501	77	60	68	2121
4040[28-29]	28.5	20016	16	82	393	78	70	63	1928
4040[29-30]	29.5	20614	19	82	401	98	122	63	1662
4040[32-34]	33	22706	18	91	425	81	59	72	2138
4040[34-36]	35	23902	17	80	395	104	128	63	1860
4040[36-38]	37	25097	18	89	413	115	139	72	2032
4040[42-44]	43	28683	16	81	361	100	131	60	1846
4040[44-46]	45	29879	18	81	355	77	72	64	2020
4040[46-48]	47	31074	18	86	406	104	123	67	1981
4040[48-50]	49	32270	19	75	421	98	118	60	1816
4040[52-54]	53	34661	18	78	323	92	120	58	1694
4040[54-56]	55	35856	17	70	402	97	137	51	1514

To ascertain the variation in sediments flux in core 4032, the flux of the detrital proxies were calculated using the varying sedimentation rate and the moisture content. The average flux of Al, Fe, Mg and Ti was found to be near constant between 50 kyr till 20 kyr with a minor increase around 40 kyr. For example, Al and Fe varied between 15–25 $\text{g.cm}^{-2}.\text{kyr}^{-1}$, Mg 4–8 $\text{g.cm}^{-2}.\text{kyr}^{-1}$ and Ti 1–2 $\text{g.cm}^{-2}.\text{kyr}^{-1}$. After 20 kyr, all the lithogenic proxies show abrupt increases that persist till 14 kyr (Al and Fe 85–90 $\text{g.cm}^{-2}.\text{kyr}^{-1}$, Mg 28 $\text{g.cm}^{-2}.\text{kyr}^{-1}$ and Ti 6 $\text{g.cm}^{-2}.\text{kyr}^{-1}$). After 14 kyr till 2 kyr, overall a decrease in all proxies was seen (Fig. 5.6). In the absence of availability of moisture measurements for the core 4040, the fluxes could not be calculated for this

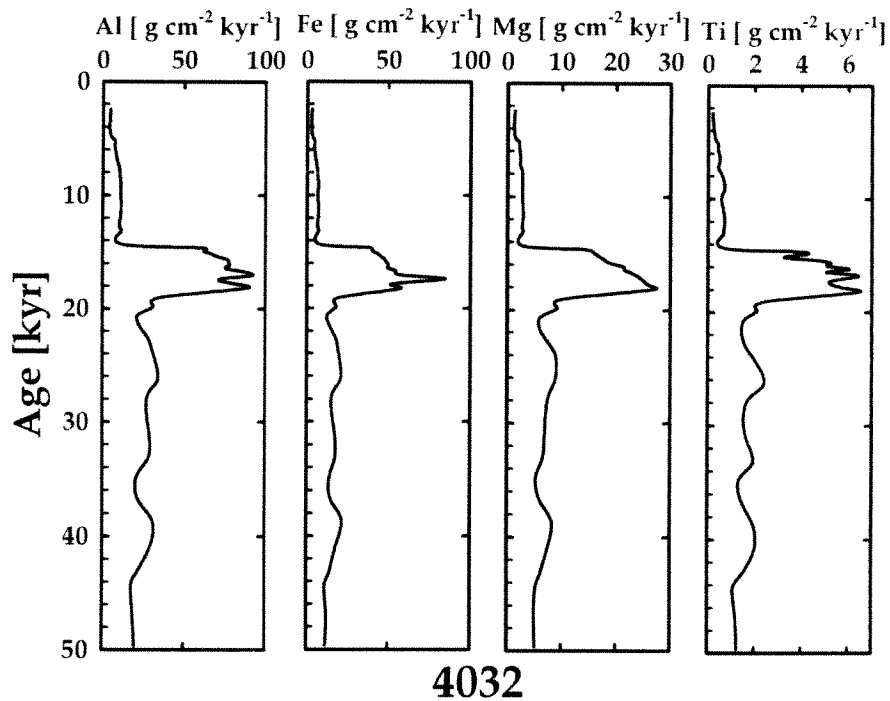


Fig. 5.6: Mass accumulation rate of lithogenic proxies for the core 4032. Abrupt increase from 20 kyr to 14 kyr indicates enhanced sediment flux.

core.

The geochemical proxies were further weight normalized to Al in order to ascertain the temporal changes in sediment provenance for both central (4032) and southern (4040) Bay of Bengal cores (Figs. 5.7 and 5.8). The reason being, weighted ratios of Ti/Al and Mg/Al has been successfully used to infer changes in the aeolian contribution through time in the western and

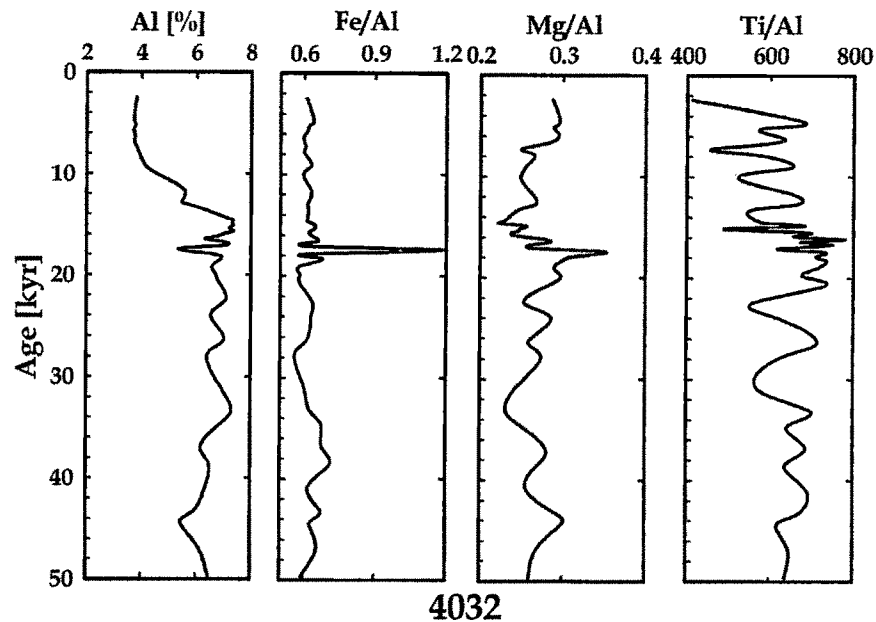


Fig. 5.7 Downcore variation of Al, Fe/Al, Mg/Al and Ti/Al in the core 4032

northwestern Arabian Sea (Sirocko et al., 1993; Reichart et al., 1997). However, in the case of southern Bay of Bengal (4040), a linear increase in Ti/Al ratio through time was attributed to increased denudation rates in Himalayan, maturation of Indian River systems and evolution of the southwest monsoon system (Nath et al., 1997; Timothy and Calvert, 1998).

The Fe/Al ratio in core 4032 remained almost constant (~ 0.6) except around 18 kyr where it sharply increases to 1. The Mg/Al ratio shows marginal fluctuation with an increase around 44 kyr and 18 kyr, following this, the ratio decreases till 12 kyr. After 12 kyr, a marginal increase is seen. In the case of Ti/Al, it can be suggested that there was an overall increase until around 18 kyr with prominent low values between ~ 34 kyr and ~ 22 kyr punctuated by an increase at ~ 26 kyr. After 18 kyr, an overall decrease with fluctuation till 2 kyr has been observed (Fig. 5.7). In the case of southern Bay of Bengal (4040), Fe/Al and Ti/Al ratios show an increasing trend from 36 kyr culminating around 30 kyr. After 30 kyr, Fe/Al show almost constant value

with minor fluctuation till 14 kyr. Following this, a marginal decrease till 1.5 kyr was seen. Similar trends are also observed in Mg/Al and Ti/Al (Fig. 5.8).

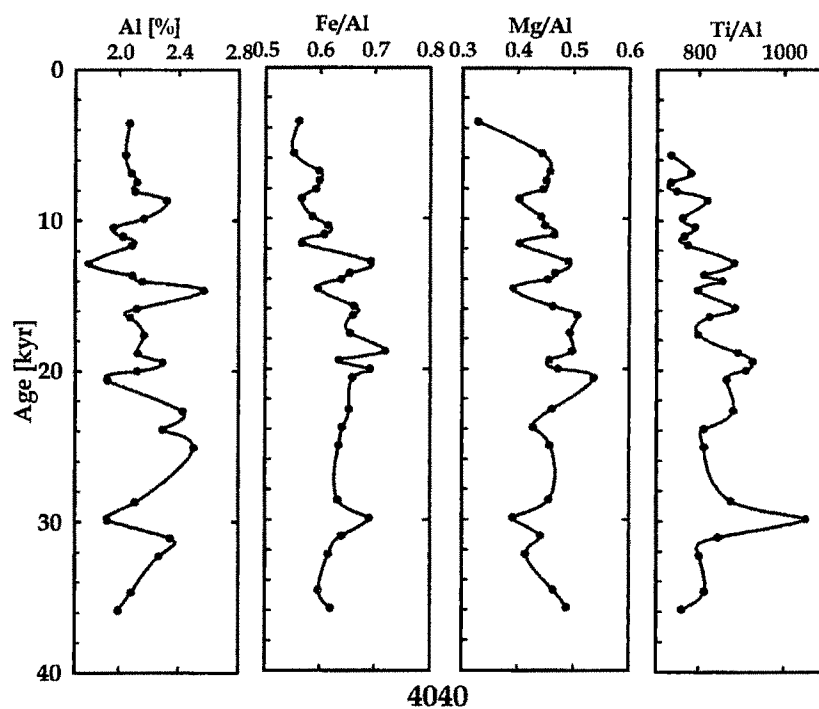


Fig. 5.8 Downcore variation of Al, Fe/Al, Mg/Al and Ti/Al in the core 4040.

Variation in Productivity Proxies

Palaeoproductivity is estimated using the biogenic remnants such as organic carbon, carbonate, opal, barium etc. Productivity in the Bay of Bengal is influenced by coastal upwelling along the east coast of India during SW monsoon (Shetye et al., 1991; Madhupratap et al., 2003; Kumar et al., 2004; Prassanna Kumar et al., 2007). The high freshwater flux from the Ganga and the Brahmaputra River in the northern region of the Bay of Bengal dampens the upwelling signatures. The primary productivity during December is marginally high (0.3 to 0.7 $\text{g.C.m}^{-2}.\text{day}^{-1}$) due to strengthened NE monsoon (October–November) that facilitates the supply of nutrients to the coastal waters. However, compared to this, the average surface productivity during SW monsoon (June–September) is relatively high which ranges from 51 to 113 $\text{mg.C.m}^{-2}.\text{day}^{-1}$ (Madhupratap et al., 2001; Gauns et al., 2005).

Carbonate, organic carbon, C/N ratio, $\delta^{13}\text{C}$, $\delta^{15}\text{N}$ along with Ca, Ba, and Sr and ratio of these elements normalized to Al were used as indicators of palaeoproductivity. The carbonate contribution in marine sediment (continental slope and pelagic oceans) is due to the growth of coccolithophores, foraminifera and pteropods. Concentration of phytoplanktons is governed by the presence of nutrients which can be of primary origin (from continent) or recycled by upwelling. In either case, variation in marine carbonate in principle would suggest strengthened monsoon conditions.

In core 4032, the carbonate concentration fluctuates around 20% between 50 kyr to ~14 kyr punctuated by frequent millennial scale low amplitude fluctuations (Table 5.4). After 14 kyr, a steady rise in carbonate content was observed that attains a maximum value of ~55% at the top dated

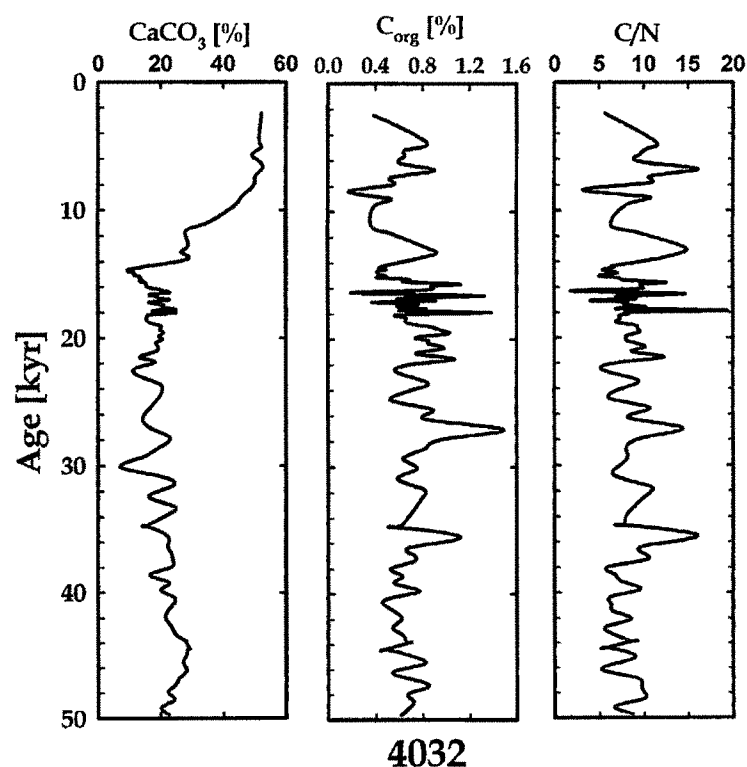


Fig. 5.9 Downcore variation of CaCO_3 , C_{org} and C/N in the core 4032

Table 5.4: Concentration of total carbon, organic carbon (C_{org}) and $CaCO_3$ along with C/N ratios in the core 4032

Core	Depth (cm)	Age (yrs)	$CaCO_3$ (%)	Total C (%)	N (%)	C_{org} (%)	C/N
4032(0-2)	1	2454	52	6.7	0.07	0.39	5.7
4032(3-4)	3.5	4595	52	7.0	0.07	0.84	11.3
4032(4-5)	4.5	5137	52	6.9	0.06	0.66	10.6
4032(5-6)	5.5	5680	49	6.6	0.07	0.65	9.5
4032(6-7)	6.5	6222	52	6.8	0.06	0.62	9.8
4032(7-8)	7.5	6765	53	7.2	0.06	0.90	16.1
4032(8-9)	8.5	7307	50	6.6	0.05	0.53	10.8
4032(9-10)	9.5	7849	50	6.6	0.05	0.56	10.7
4032(10-11)	10.5	8392	49	6.0	0.05	0.17	3.1
4032(11-12)	11.5	8934	46	6.0	0.05	0.52	10.4
4032(12-13)	12.5	9476	44	5.7	0.05	0.40	8.3
4032(13-15)	14	10290	40	4.7	0.05	--	--
4032(15-16)	15.5	11104	34	4.4	0.06	0.37	6.4
4032(16-17)	16.5	11646	28	3.9	0.06	0.52	8.8
4032(18-19)	18.5	12731	29	4.3	0.06	0.82	14.1
4032(19-20)	19.5	13273	27	4.1	0.06	0.91	14.4
4032(20-21)	20.5	13816	29	4.1	0.06	0.67	11.4
4032(21-22)	21.5	14358	16	2.3	0.07	0.43	6.7
4032(22-23)	22.5	14488	14	2.1	0.07	0.49	6.7
4032(23-24)	23.5	14617	10	1.6	0.07	0.42	5.7
4032(24-25)	24.5	14747	10	1.6	0.07	0.42	5.7
4032(25-26)	25.5	14877	12	1.8	0.06	0.44	7.1
4032(26-27)	26.5	15006	11	1.9	0.08	0.49	5.9
4032(27-28)	27.5	15136	13	2.0	0.08	0.42	5.1
4032(28-29)	28.5	15265	13	2.3	0.10	0.68	6.8
4032(29-30)	29.5	15395	14	2.3	0.09	0.64	7.5
4032(30-31)	30.5	15525	13	2.4	0.09	0.76	8.8
4032(31-32)	31.5	15654	15	2.9	0.09	1.12	12.6
4032(32-33)	32.5	15784	15	2.7	0.09	0.91	10.1
4032(33-34)	33.5	15914	15	2.7	0.09	0.89	9.8
4032(34-35)	34.5	16043	17	2.9	0.09	0.87	9.7
4032(35-36)	35.5	16173	20	3.1	0.08	0.69	8.8
4032(36-37)	36.5	16302	21	2.7	0.11	0.20	--
4032(37-38)	37.5	16432	23	3.4	0.08	0.63	8.0
4032(38-39)	38.5	16562	17	3.3	0.09	1.33	14.7
4032(39-40)	39.5	16691	19	3.1	0.09	0.81	8.9
4032(40-41)	40.5	16821	19	2.9	0.09	0.61	7.2
4032(41-42)	41.5	16951	23	3.6	0.10	0.90	9.0
4032(42-43)	42.5	17080	20	2.8	0.09	0.37	4.0
4032(43-44)	43.5	17210	16	2.7	0.10	0.76	8.0
4032(44-46)	45	17404	21	3.1	0.07	0.58	7.8
4032(46-47)	46.5	17599	21	3.3	0.08	0.83	10.2
4032(47-48)	47.5	17728	25	3.6	0.08	0.62	7.4
4032(48-49)	48.5	17858	17	3.5	0.07	1.38	19.4
4032(49-50)	49.5	17988	25	3.8	0.09	0.80	9.4
4032(50-51)	50.5	18117	18	2.7	0.07	0.57	8.3
4032(51-52)	1.5	18247	16	2.5	0.09	0.65	7.3
4032(52-53)	52.5	18508	15	2.5	0.09	0.66	7.4
4032(53-54)	53.5	18769	1719.9	2.7	0.10	0.71	7.0

4032(54-55)	54.5	19031	19.6	3.27	0.10	0.88	9.1
4032(55-56)	55.5	19292	20.9	3.31	0.10	0.96	9.3
4032(56-57)	56.5	19553	19.3	3.52	0.11	1.01	9.5
4032(57-58)	57.5	19814	20.5	3.06	0.09	0.75	8.2
4032(58-59)	58.5	20076	18.5	3.30	0.11	0.84	8.0
4032(59-60)	59.5	20337	19.2	3.07	0.10	0.85	8.5
4032(60-61)	60.5	20720	17.6	3.28	0.10	0.98	10.2
4032(61-62)	61.5	21103	13.4	2.85	0.09	0.74	8.7
4032(62-63)	62.5	21486	18.2	2.68	0.09	1.07	12.3
4032(63-64)	63.5	21870	11.3	2.95	0.10	0.77	8.1
4032(64-66)	65	22444	15.9	1.92	0.11	0.57	5.3
4032(66-68)	67	23211	20.5	2.70	0.09	0.80	9.0
4032(68-70)	68.5	23786	19.1	3.24	0.09	0.78	8.5
4032(70-72)	71	24744	16.4	2.82	0.09	0.53	6.1
4032(72-74)	73	25510	14.3	2.87	0.08	0.89	10.8
4032(74-76)	75	26276	16.8	2.54	0.10	0.83	8.3
4032(76-78)	77	27043	23.0	3.51	0.10	1.49	14.3
4032(78-80)	79	27809	19.3	3.75	0.10	0.98	10.2
4032(80-82)	81	28576	13.9	3.13	0.10	0.82	8.1
4032(82-84)	83	29342	7.3	2.30	0.08	0.63	8.2
4032(84-86)	85	30108	21.0	1.63	0.11	0.75	7.1
4032(86-88)	87	30875	23.0	3.10	0.09	0.59	6.9
4032(88-90)	89	31641	16.1	3.55	0.07	0.79	10.6
4032(90-92)	91	32408	24.5	2.73	0.08	0.80	10.2
4032(92-94)	93	33174	21.1	2.37	0.09	--	--
4032(94-96)	95	33940	15.2	3.21	0.08	0.68	8.1
4032(96-98)	97	34707	21.9	2.40	0.08	0.58	7.8
4032(98-100)	99	35473	22.2	3.75	0.07	1.12	16.0
4032(100-102)	101	36240	23.3	3.38	0.07	0.72	10.7
4032(102-104)	103	36824	23.9	3.51	0.07	0.71	9.8
4032(104-106)	105	37407	22.8	3.59	0.07	0.72	10.3
4032(106-108)	107	37991	16.5	3.26	0.09	0.52	6.0
4032(108-110)	109	38574	22.7	2.61	0.09	0.63	6.8
4032(110-112)	111	39158	19.9	3.28	0.07	0.56	7.6
4032(112-114)	113	39741	24.1	3.16	0.08	0.77	9.6
4032(114-116)	115	40325	23.9	3.40	0.08	0.51	6.4
4032(116-118)	117	40908	21.9	3.35	0.08	0.48	6.4
4032(118-120)	119	41492	21.6	3.22	0.09	0.59	6.7
4032(120-122)	121	42075	23.4	3.20	0.07	0.61	8.6
4032(122-124)	123	42658	24.7	3.35	0.09	0.55	5.9
4032(124-126)	125	43242	28.1	3.60	0.10	0.64	6.5
4032(126-128)	127	43825	28.8	4.04	0.08	0.67	8.6
4032(128-130)	129	44409	28.1	3.96	0.08	0.51	6.2
4032(130-132)	131	44992	27.1	4.10	0.08	0.73	9.0
4032(132-134)	133	45576	28.3	4.05	0.11	0.80	7.3
4032(134-136)	135	46159	25.9	3.95	0.10	0.55	5.3
4032(136-138)	137	46743	24.7	3.80	0.08	0.69	8.9
4032(138-140)	139	47326	22.3	3.81	0.09	0.85	9.8
4032(140-142)	141	47910	24.4	3.35	0.07	0.68	10.0
4032(142-144)	143	48493	20.2	3.64	0.07	0.72	9.9
4032(144-146)	145	49077	22.5	3.10	0.10	0.68	6.7
4032(146-148.5)	147	49660		3.31	0.07	0.61	8.7

to 2.5 kyr (Fig. 5.9). Compared to this in core 4040, a gradual increase in carbonate concentration is observed after 40 kyr followed by a declining trend culminating around 30 kyr. Further, a marginal increase is noticed after 22 kyr with fluctuations followed by an increasing trend after 14 kyr which peak around 12.5 kyr. After 12.5 kyr, a marginal decline in carbonate concentration was observed which persists till 7 kyr. After 7 kyr till 3 kyr, it shows an increasing trend (Fig. 5.10).

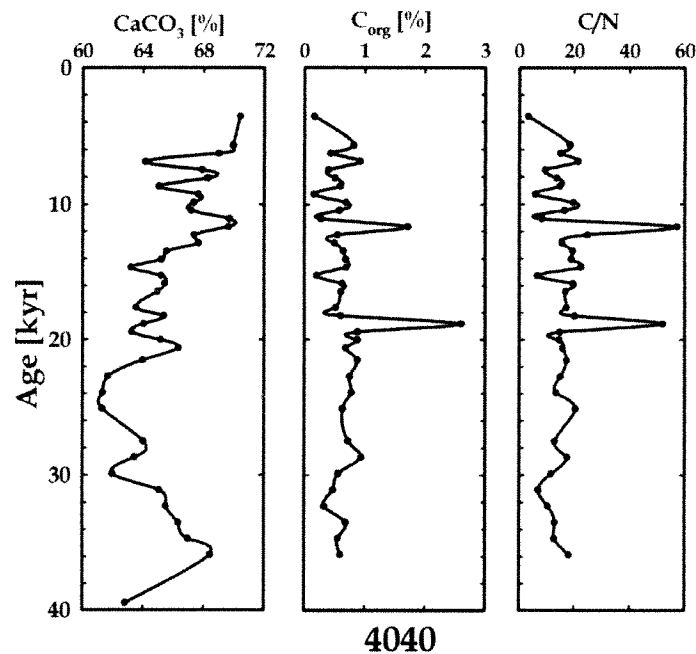


Fig. 5.10 Downcore variation of CaCO_3 , C_{org} and C/N in the core 4040

Though, there are several factors controlling the sedimentary organic carbon (C_{org}), it has still been extensively used to estimate palaeoproductivity (Agnihotri et al., 2003b; Bhushan et al., 2001; Galy et al., 2008). In the open ocean, only a small fraction of the organic matter produced in the upper ocean surface reaches the sea floor due to the degradation by microbial and chemical processes while it descends to the seafloor. However, on reaching the sea floor, early diagenetic reactions at sediment water interface makes it refractory and hence it gets preserved in the sediment record (Hartnett et al., 1998). Although, C_{org} in coastal regions can be used as a productivity indicator, the C_{org} content variation in the open ocean is due to its

preservation characteristics. In view of this, C_{org} has limited applicability as a potential productivity tracer in the open ocean (Emerson, 1985; Emerson and Hedges, 1988; Calvert and Pedersen, 1992; Paropkari et al., 1993; Canfield, 1994; Hartnett et al., 1998).

C_{org} in both the cores remained fairly constant (fluctuation between 0.5 to 1%) except for an increase around 35.5 kyr, 27 kyr and 18 kyr (core 4032) and around 20 kyr and 12 kyr (core 4040). During these periods, the C_{org} value is >1% (Table 5.5, Figs. 5.9 and 5.10). The carbon/nitrogen (C/N) ratio in the marine sediments is used to trace the source of organic carbon. For instance, the reported C/N ratio of phytoplankton and zooplankton is ~6, for freshly deposited organic matter, this ratio is ~10, while terrigenously (land derived) derived organic matter has ratios ranging from 20–200 (Meyers 1994, 1997). Overall the C/N ratio fluctuates between 5–10 suggesting a predominantly marine origin of the organic matter (overhead productivity). However, there are periods viz. 35.5 kyr, 27 kyr, 18 kyr, 13 kyr and 7 kyr (core 4032) and 20 kyr, 12 kyr (core 4040) when C/N ratio is greater than 10 (Figs. 5.9 and 5.10) suggesting a continental source. The $\delta^{13}C$ of the organic matter in marine sediments is used to identify the continental versus marine source of the organic matter. The marine organic matter $\delta^{13}C$ is around -19‰ , whereas for the continental origin it is around -26‰ (Table 5.6). The $\delta^{13}C$ of the organic matter in the northern Bay of Bengal (core 4032) is modulated by both overhead productivity and its subsequent enhanced transport to seafloor by adhering to the detrital particles from continental input (France–Lanord and Derry, 1994; Galy and France–Lanord, 2006; Galy et al., 2008). It is observed in core 4032 that during 42 kyr and 16 kyr, the $\delta^{13}C$ values fluctuated between -20‰ and -18‰ implying the dominance of marine origin material. After 16 kyr, depleted value of $\delta^{13}C$ ($<-22\text{‰}$) suggests a continental organic carbon contribution (Fig. 5.11).

The $\delta^{15}N$ of the C_{org} reflects the denitrification process in the marine sediments. The C_{org} undergoes microbial degradation through consumption of

Table 5.5: Concentration of total carbon, organic carbon (C_{org}) and CaCO₃ along with C/N ratios in the core 4040.

Core	Depth (cm)	Total C (%)	CaCO ₃ (%)	N (%)	C _{org} (%)	C/N
4040 [0-2]	1	8.6	70	0.05	0.16	3.3
4040 [4-5]	4.5	9.2	70	0.04	0.82	18.5
4040 [5-6]	5.5	8.7	69	0.03	0.43	15.0
4040 [6-7]	6.5	8.6	64	0.04	0.92	21.5
4040 [7-8]	7.5	8.6	68	0.04	0.40	9.5
4040 [8-9]	8.5	8.7	68	0.04	0.51	13.7
4040 [9-10]	9.5	8.4	65	0.04	0.59	14.9
4040 [10-11]	10.5	8.3	68	0.03	0.15	5.9
4040 [11-12]	11.5	8.8	67	0.04	0.69	19.7
4040 [12-13]	12.5	8.6	67	0.04	0.58	16.6
4040 [13-14]	13.5	8.6	70	0.03	0.28	8.4
4040 [14-15]	14.5	10.1	70	0.03	1.71	57.1
4040 [15-16]	15.5	8.6	67	0.02	0.55	24.9
4040 [16-17]	16.5	8.6	68	0.03	0.50	15.7
4040 [17-18]	17.5	8.5	66	0.03	0.65	19.6
4040 [18-19]	18.5	8.5	65	0.04	0.68	19.0
4040 [19-20]	19.5	8.3	63	0.03	0.69	22.4
4040 [20-21]	20.5	8.0	65	0.03	0.20	6.7
4040 [21-22]	21.5	8.5	65	0.03	0.63	19.6
4040 [22-23]	22.5	8.4	65	0.04	0.61	16.8
4040 [24-25]	24.5	8.1	64	0.03	0.52	17.2
4040 [26-27]	26.5	8.3	64	0.03	0.61	20.2
4040 [27-28]	27.5	10.2	63	0.05	2.60	52.0
4040 [28-29]	28.5	8.7	65	0.06	0.88	14.9
4040 [29-30]	29.5	8.8	66	0.06	0.88	14.7
4040 [30-32]	31	8.4	64	0.04	0.68	15.9
4040 [32-34]	33	8.3	62	0.05	0.88	17.3
4040 [34-36]	35	8.1	61	0.05	0.75	15.0
4040 [36-38]	37	8.1	61	0.06	0.78	13.5
4040 [40-42]	41	8.3	64	0.03	0.64	20.5
4040 [42-44]	43	8.3	63	0.06	0.73	13.0
4040 [44-46]	45	8.4	62	0.05	0.94	17.5
4040 [46-48]	47	8.4	65	0.05	0.56	11.7
4040 [48-50]	49	8.3	66	0.07	0.48	7.1
4040 [50-52]	51	8.3	66	0.03	0.33	10.6
4040 [52-54]	53	8.7	67	0.05	0.69	13.1
4040 [54-56]	55	8.8	68	0.04	0.56	13.0
4040 [60-62]	61	8.1	63	0.03	0.60	18.2

Table 5.6: $\delta^{13}\text{C}$ and $\delta^{15}\text{N}$ of the organic matter in the core 4032 from the Bay of Bengal.

Core	Depth (cm)	Age (yrs)	$\delta^{13}\text{C}$ (‰)	$\delta^{15}\text{N}$ (‰)
4032(0-2)	1	2000	-20.2	6.2
4032(3-4)	3.5	4876	-20.9	--
4032(7-8)	7.5	7050	-19.9	--
4032(11-12)	11.5	9224	-22.0	5.7
4032(16-17)	16.5	11941	-22.3	--
4032(21-22)	21.5	14658	-21.5	4.3
4032(23-24)	23.5	15280	-21.2	--
4032(27-28)	27.5	16522	-21.2	4.4
4032(31-32)	31.5	17764	-20.3	4.6
4032(35-36)	35.5	19007	-22.9	--
4032(39-40)	39.5	20248	-18.4	5.0
4032(44-46)	45	20869	-18.0	5.1
4032(53-54)	53.5	20869	-20.7	--
4032(60-61)	60.5	21532	-21.1	--
4032(64-66)	65	24512	-18.7	4.5
4032(72-74)	73	29148	-19.2	5.2
4032(82-84)	83	33899	-18.8	4.7
4032(92-94)	93	35059	-20.2	4.8
4032(102-104)	103	36295	-17.8	5.0
4032(112-114)	113	39372	-18.8	4.7
4032(124-126)	125	43065	-21.3	--
4032(128-130)	129	44295	-21.3	--
4032(136-138)	137	46755	-19.7	5.2
4032(146-148.5)	147	49834	-21.9	--

the dissolved oxygen while it's traverse through the water column. Enhanced overhead productivity results in depletion of the dissolved oxygen in the sub-surface waters causing an Oxygen Minimum Zone (200–1000 m) within the water column due to its consumption by C_{org} , as a result there is a reduction of nitrate to nitrite and finally to N_2 (Naqvi, 1994; Howell et al., 1997; Naqvi et al., 2006). This process of oxygen consumption by the settling C_{org} material is known as denitrification. The process of denitrification leads to an enrichment of $\delta^{15}N$ of the C_{org} with increasing denitrification (Schafer and Ittekkot, 1993; Altabet et al., 2002). The $\delta^{15}N$ values vary narrowly between 4 ‰ to 5.2 ‰ between 50 kyr to 14 kyr. After 14 kyr, a steady increase up to 6‰ indicates an intensification of the denitrification process (Fig. 5.11).

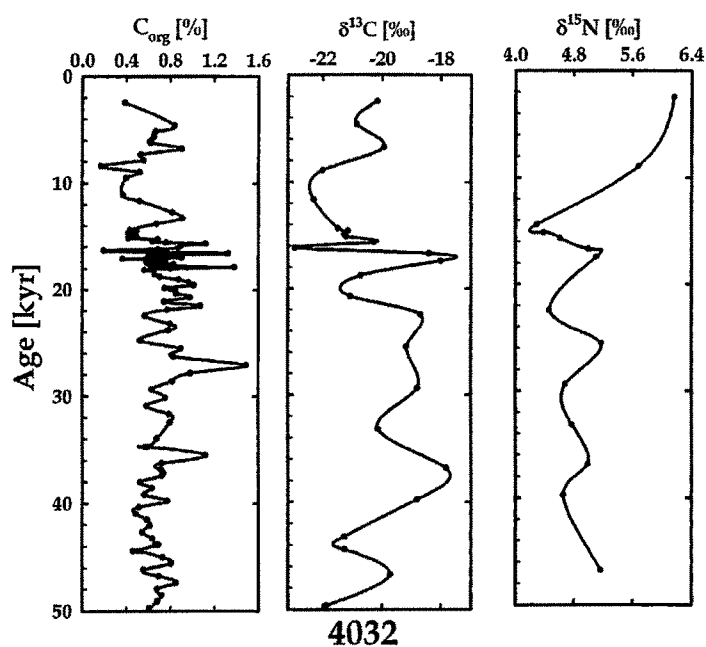


Fig. 5.11: Downcore variation of C_{org} and $\delta^{13}C$ and $\delta^{15}N$ of the organic matter in the core 4032.

Only 0.1 to 1% of the organic carbon produced in the surface waters is preserved in sediments (Berger et al., 1989), therefore, palaeoproductivity estimates based on organic carbon is fraught with uncertainties (Klump et al., 2000). In view of this, the variation in productivity based on organic carbon as

discussed above is further assessed using geochemical proxies as Ba, Ca and Sr, which are considered to be less affected by post depositional changes (Dymond et al., 1992; Schenau et al., 2001; Babu et al., 2002).

Barium is supplied to the seafloor by two main sources (i) within silicate lattice of terrigenous material and (ii) in association with organic matter as barite (Pattan et al., 2003). Ba enrichment is found in the sediments underneath the high biological productivity areas of coastal upwelling and in the equatorial divergent zones (Goldberg and Arrhenius, 1958). Barium is a useful proxy of surface ocean productivity in the overlying water column due to its high preservation factor as compared to its production (Bishop, 1988; Goldberg and Arrhenius, 1958; Schmitz, 1987). Algorithms have been developed to link biogenic barium accumulation in sediment to export production from water column (Dymond et al., 1992; Francois et al., 1995). Since the formation of barite is mechanically linked to biogenic material, biogenic Ba or Ba/Al ratio can be used as an indicator of surface productivity (Dymond, et al., 1992; Sirocko et al., 1996), provided the core location is free from reducing environment effects that can cause diagenetic dissolution (McManus et al., 1998). Both central and southern Bay of Bengal cores are raised from deep water, much below the denitrification zone (~ 200–700 m), and hence are less likely to be effected by reduction processes. The calcium in the cores is mostly derived from the overhead calcareous productivity of foraminifer species. Additionally, due to significant lithogenic flux in the Bay of Bengal, a fraction of Ca is likely to be associated with the dolomitic material brought along with the detrital material. Similarly, Sr with similar ionic radii gets incorporated in the calcareous material of the foraminifers and contributes for the major fraction of the Sr in sediments (Derry and France-Lanord, 1996). However, a significant fraction of Sr is expected to be associated with the silicate and the calcite fraction of the material delivered to the Bay of Bengal from various rivers (Krishnaswami et al., 1992; Bickle et al., 2005; Hohndorf et al., 2003).

The overhead productivity was ascertained using the variation in the concentration of Ba, Ca and Sr normalized to Al (Figs. 5.12 and 5.13). In core 4032, a marginal increase in Ca/Al, Ba/Al and Sr/Al is observed between 48 kyr to 42 kyr, followed by a consistent ratio (low) till around 14 kyr. After 14 kyr, a steady increase in all the proxies is observed which culminates around 7.5 kyr. After 7.5 kyr to 2 kyr, Ca/Al and Sr/Al show constant ratio (high), whereas, Ba/Al show a decreasing trend (Fig. 5.12).

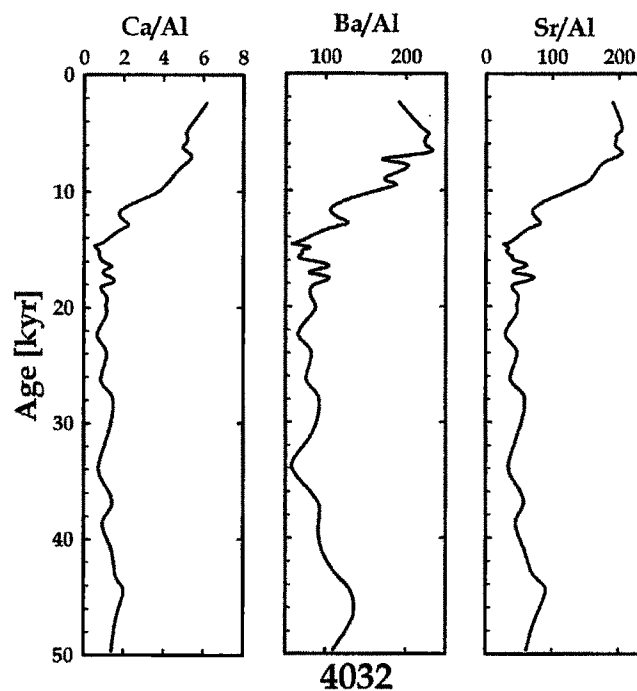


Fig. 5.12: Downcore variation of Ca/Al, Ba/Al and Sr/Al in the core 4032.

In core 4040, except for Ba/Al, both Ca/Al and Sr/Al show significant variability during 36 kyr and 4 kyr (Fig. 5.13). All the above proxies show a decreasing trend between 36 kyr to around 32 kyr, followed by an increase around 30 kyr. This increase is succeeded by an overall decreasing trend till 22 kyr. After 22 kyr, an abrupt increase is observed between 22 kyr and 20 kyr for Ca/Al and Sr/Al ratio, whereas, Ba/Al shows a marginal increasing trend. After 20 kyr, a general increase in all the proxies Ca/Al, Ba/Al and Sr/Al is observed with fluctuations with a sharp decline in all of them at 14.5 kyr. After 10 kyr, a declining trend is noticed with an abrupt decrease near 8.5

kyr followed by a marginal increase. However, in case of Ba/Al ratio, a gradual increase with minor fluctuations was observed after 20 kyr which continues till 4 kyr (Fig. 5.13).

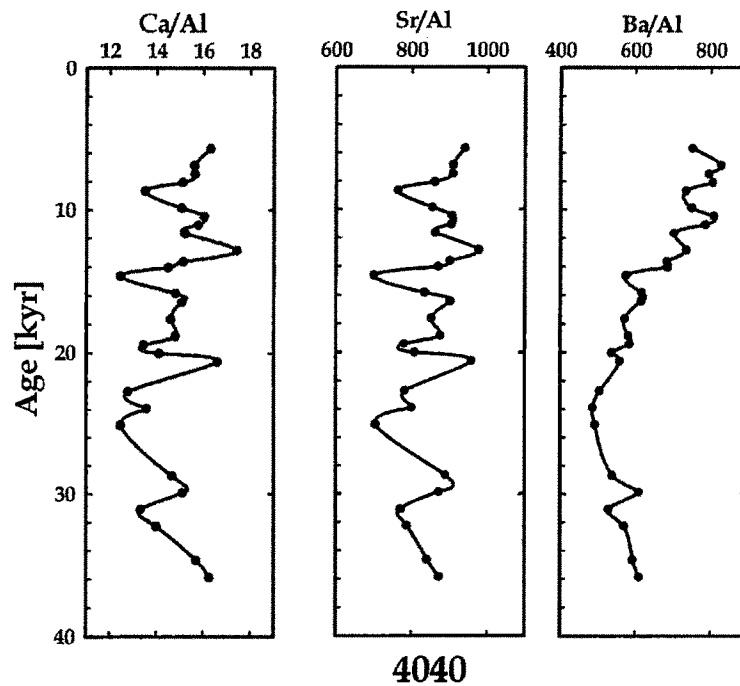


Fig. 5.13: Downcore variation of Ca/Al, Ba/Al and Sr/Al in the core 4040.

Variation in Trace Element Proxies

The trace elements in deep sea sediments have characteristically different composition as compared to the continental and near shore sediments. The deep-sea clays are enriched in certain trace elements (e.g. Mn, Cu) compared to the near shore and continental sediments (Chester and Hughes, 1969). The chemical composition of the deep sea is governed by the relative proportion of the minerals, pathways of its delivery in the marine environment, mechanism of its incorporation and sedimentation pattern (Wedepohl, 1960; Turekian and Wedepohl, 1961; Bostrom et al., 1973). Marine sedimentation is modulated by the rate of terrigenous flux (continental) and biogenic productivity variations. Post-depositional changes are governed by the ambient environmental conditions (changes in oxidizing conditions). For example, preservation of organic carbon was observed during reducing

conditions in the anoxic waters of the Oxygen Minimum Zone (OMZ) on the western continental slope of India (Sirocko et al., 2000; van der Weijden et al., 2006). The sediments in contact with OMZ have an absence of benthonic metazoan life due to oxygen depletion, eventually ceasing bioturbation and ultimately resulting in well preserved hydrogen-rich organic matter and have excellent hydrocarbon generation potential (Paropkari et al., 1993).

Unlike other open ocean regimes, the Bay of Bengal sediments provide a mixed signature of various proxies due to different processes operating in this region. The Bay of Bengal experiences temporal changes in the overhead productivity due to seasonally reversing monsoon system along with changes in the flux of detrital materials contributed by various rivers. Mn, Cr and V are redox sensitive elements which tend to migrate or get enriched in certain

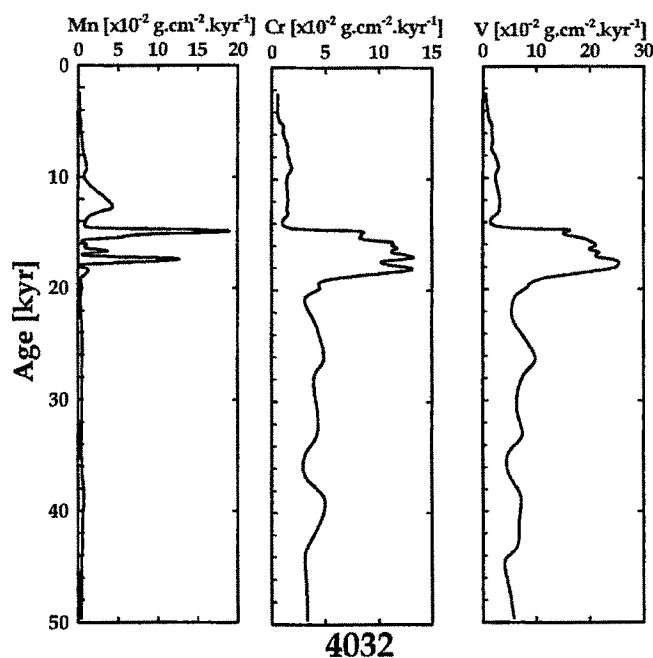


Fig. 5.14: Downcore variation of fluxes of redox sensitive elements in core 4032.

regions depending on the prevailing redox conditions governed either due to (i) changing overhead productivity (ii) varying sedimentation rates and/or (iii) changing bottom water conditions (Yadav, 1996; Chauhan and Rao., 1999; Chauhan, 2003). Redox sensitive elements thus provide information about the

changing bottom water conditions. However, if the trace elements are normalized to Al, the ratios would mimic the redox conditions caused due to the changing overhead productivity (Mangini et al., 2001). In core 4032, V and Cr show marginal variation in the fluxes between 50 kyr to 20 kyr (V 3–5 g.cm².kyr⁻¹ and Cr 5–10 g.cm².kyr⁻¹). Between 20 kyr and 14 kyr, these redox sensitive trace elements show significant increase in their fluxes. Compared to this, Mn shows only two distinct sharp peaks around 18 kyr and 14 kyr and

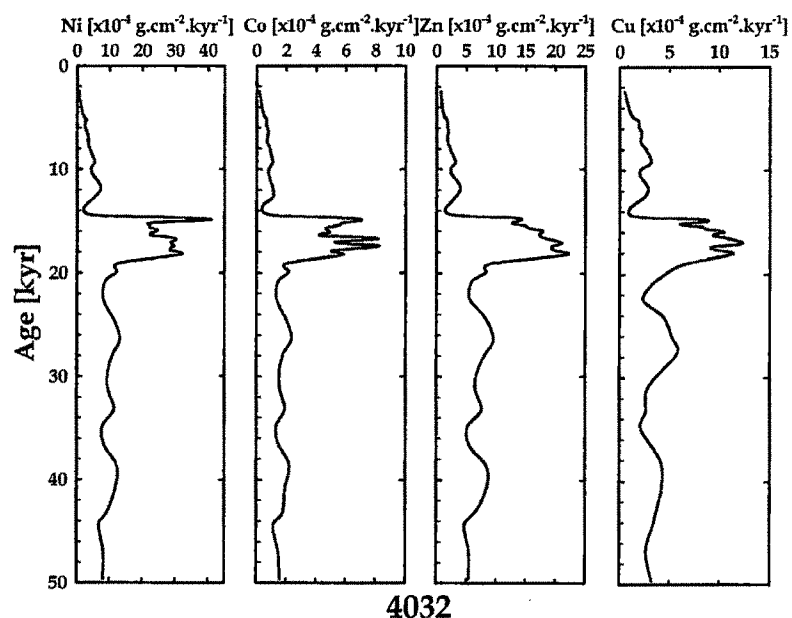


Fig 5.15: Downcore variation of fluxes of trace elemental proxies of Ni, Co, Zn and Cu in the core 4032

for the rest, it remains close to zero (Fig. 5.14). Similar trends are noticed in the fluxes of all the trace elements viz. Ni, Co, Zn and Cu measured in the core 4032 with a relatively constant flux during 50 kyr to 20 kyr and then sudden enhancement during 20 kyr to 14 kyr, but after 14 kyr all of them showed a decreasing trend (Fig. 5.15).

The redox proxies (V/Al and Cr/Al) when normalized to Al in core 4032, show a marginal increase between 50 kyr and 36 kyr. Cr/Al remain constant till 16 kyr followed by a decrease till 10 kyr. After 10 kyr, an increase till 7 kyr followed by a decreasing trend. V/Al broadly show an identical

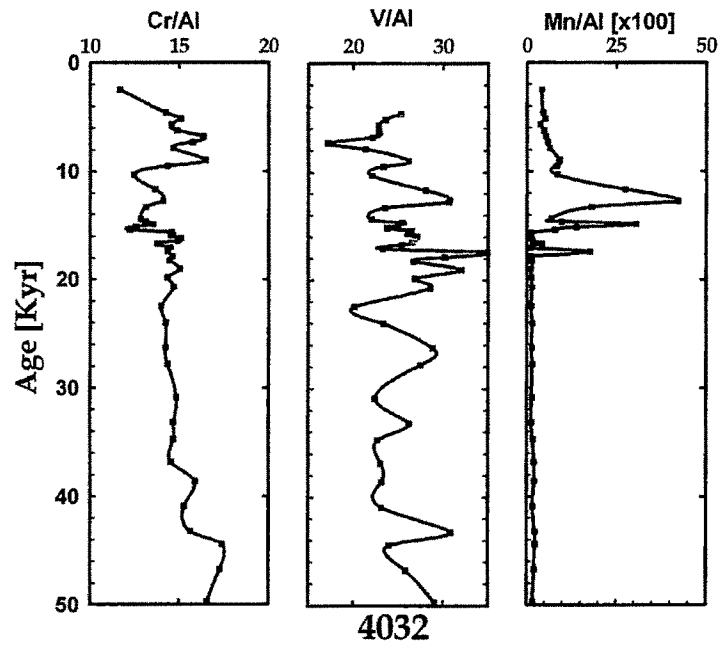


Fig. 5.16: Downcore variation of the redox sensitive elements normalized to Al for the core 4032.

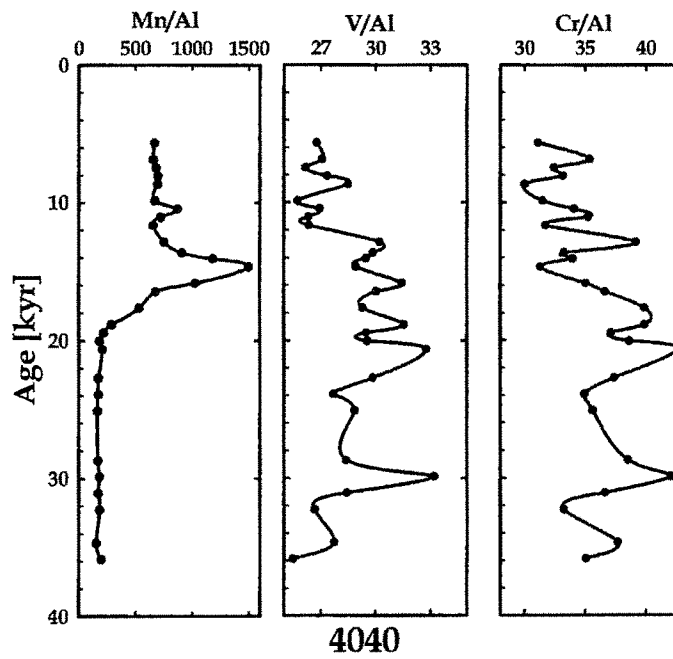


Fig. 5.17: Downcore variation of redox proxies normalised to Al in the core 4040.

pattern except for a prominent low around 22 kyr and a discernable increase during 20 kyr and 18 kyr. Whereas, Mn/Al shows a near zero

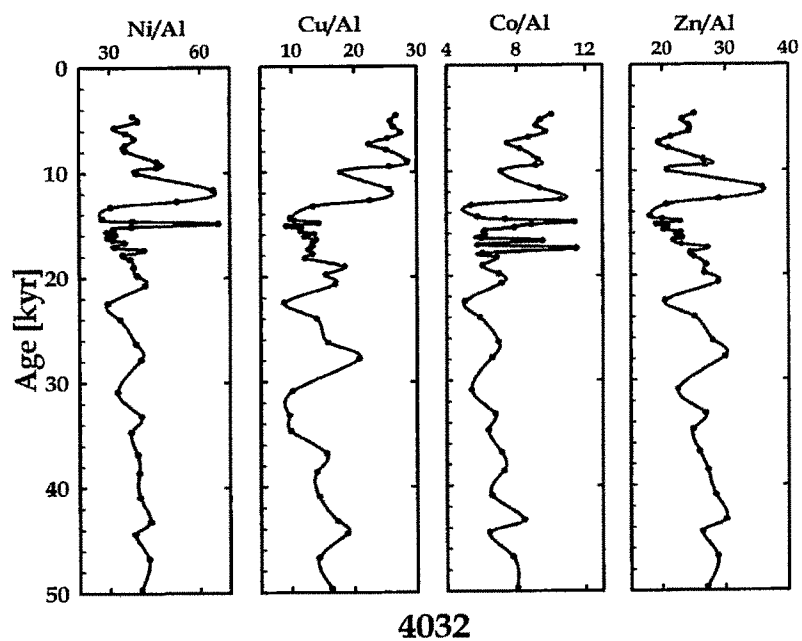


Fig. 5.18: Downcore variation of trace element proxies normalised to Al in the core 4032.

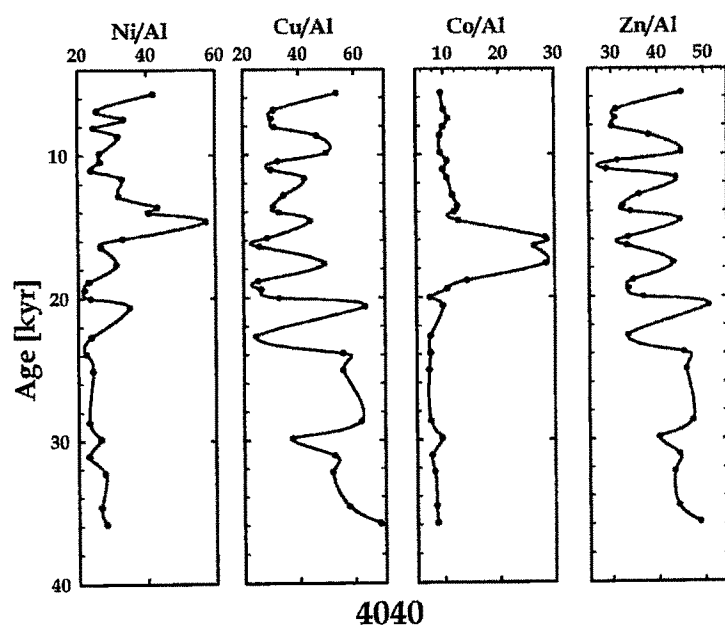


Fig. 5.19: Downcore variation of trace element proxies normalised to Al in the core 4040.

constant value through out, except for two enhanced peaks at 14 kyr and 16 kyr (Fig. 5.16).

In case of core 4040, an increasing trend between 35 kyr to 20 kyr followed by a continuous decreasing trend was observed for V/Al and Cr/Al, while Mn/Al shows a consistent low value till 19 kyr followed by a peak around 14 kyr (Fig. 5.17). When normalized with Al, Cu/Al, Co/Al and to some extent Zn/Al show an overall decreasing trend with fluctuations between 50 kyr and 20 kyr followed by an increase particularly after 14 kyr in core 4032. However, in case of Ni/Al the trend between 50 kyr and 20 kyr remains identical to that of other proxies but after 14 kyr and 10 kyr it shows a declining trend (Fig. 5.18). Similarly, an overall decreasing trend is observed in Cu/Al and Zn/Al in the core 4040 with major fluctuations and with significant enhancements at 20 kyr, 18–14 kyr and 9 kyr. Whereas, Ni/Al and Co/Al do not show any major fluctuations or trend, rather they are constant but show significant enhancement during the period 20–14 kyr (Fig. 5.19).

Strontium and Neodymium Isotopic Variations

The strontium and neodymium isotopic composition of the silicate fraction in the marine sediments preserve the record of provenance and hence that of environmental change (Raymo et al., 1988; Derry and France-Lanord, 1996, 1997; Colin et al., 1999; Burton and Vance, 2000; Clift et al., 2002; Frank, 2002). The sediments of the Bay of Bengal derive their origin to the Himalaya, Peninsular India and the Indo-Burman ranges. They have distinct Sr and Nd isotopic signatures typical to the source areas (France-Lanord et al., 1993; Singh and France-Lanord 2002; Colin et al., 2006). For example, the sediments of the G-B River system have high radiogenic $^{87}\text{Sr}/^{86}\text{Sr}$ values compared to that of the rivers draining the peninsular and Indo-Burman region. Among the G-B River system, the Ganga supplies sediments with high $^{87}\text{Sr}/^{86}\text{Sr}$ compared to the Brahmaputra. Similarly, the Nd isotopic composition of the sediments of the G-B River system (ϵ_{Nd} -12 to -18), Peninsular Rivers (-12 to -16) and Indo-Burman region (-8 to -11) are

completely distinct with enriched ϵ_{Nd} values for the Peninsular Rivers in the western Arabian Sea and that of Irrawaddy River draining through Arakan coast in the eastern Arabian Sea. Sr along with Nd isotopic composition measured in the silicate fraction of the surface sediments of the northern Bay of Bengal shows a strong influence of the G-B River system (Table 5.7; Bouquillon et al. 1990; Colin et al., 2006; Ahmad et al., 2005). Whereas, samples from the western Bay of Bengal show mixed signature of Sr and Nd isotopes derived mainly from the rivers draining the western continental margin of India (Colin et al., 1999). In case of the Andaman Sea sediments, low radiogenic Sr and more radiogenic ϵ_{Nd} , was found indicating contribution from the Irrawaddy River (Bouquillon et al., 1990; France-Lanord et al., 1993).

Table 5.7: $^{87}Sr/^{86}Sr$ and Sr concentration in the core 4032.

Core 4032	Depth (cm)	Age (yrs)	Sr (ppm)	$^{87}Sr/^{86}Sr$
0-1cm	0.5	2454	174	0.7172
5-6cm	5.5	5680	138	0.7165
16-17cm	16.5	11646	110	0.7178
21-22cm	21.5	14358	137	0.7160
25-26cm	25.2	14877	112	0.7175
31-32cm	31.5	15654	118	0.7172
35-36cm	35.5	16173	120	0.7183
39-40cm	39.5	16691	104	0.7187
42-43cm	42.5	17080	111	0.7183
51-52cm	51.5	18247	109	0.7186
55-56cm	55.5	19292	142	0.7159
64-66cm	65	22636	98	0.7190
74-76cm	75	26276	97	0.7187
78-80 cm	79	27809	120	0.7173
92-94 cm	93	33174	95	0.7184
108-110	109	38574	100	0.7187
116-118	117	40908	117	0.7179
124-126	125	43242	143	0.7164

Towards ascertaining the temporal changes in the provenance of the sediment, the silicate fraction of the sediments from the core 4032 (central Bay of Bengal) was analyzed for their Sr and Nd isotopic composition. With the same objective, the Nd isotopic composition of the sediments from the core 4040 was analysed in their silicate fraction at different depths. Selection of the sample was done on the basis of major variability observed in the proxies used for detrital flux. The measured $^{87}\text{Sr}/^{86}\text{Sr}$ in the sediments of the core 4032 varied from 0.716 to 0.719 with majority of the $^{87}\text{Sr}/^{86}\text{Sr}$ values generally remained between 0.718–0.719. Low $^{87}\text{Sr}/^{86}\text{Sr}$ values were

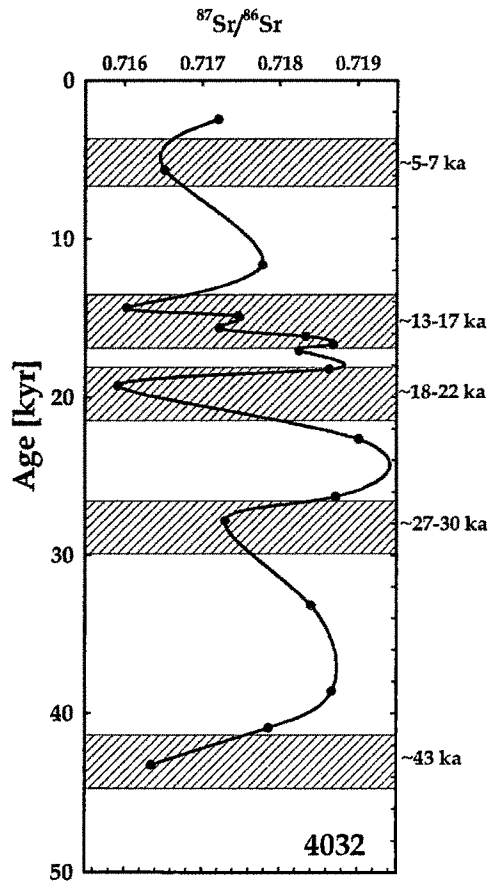


Fig. 5.20 Downcore variation of $^{87}\text{Sr}/^{86}\text{Sr}$ in the core 4032. Three prominent low $^{87}\text{Sr}/^{86}\text{Sr}$ ratios at 14, 20 and 43 kyr are observed.

observed at 6 kyr, 14 kyr, 20 kyr, 28 kyr and 43 kyr (Fig. 5.20). A close correspondence between the detrital proxies and Sr isotopic variation is seen.

The Nd isotopic composition (ϵ_{Nd}) in the sediments of the core 4032 varies between -10 and -8.9 with a general increasing pattern from 38 kyr to 20 kyr and subsequent decrease from 20 kyr to 12 kyr. There are three distinct events of increase in ϵ_{Nd} in core 4032 around 16 kyr, 20 kyr and 33 kyr. Out of these, a major increase is observed around 20 kyr (ϵ_{Nd} of -8.9) (Fig. 5.21). In core 4040, the Nd isotopic composition shows a gradual increase from 32 kyr (ϵ_{Nd} -10.5) and culminates around 20 kyr (ϵ_{Nd} -8.0). After 20 kyr, till 10 kyr a

decreasing trend of ϵ_{Nd} is noticed followed by a marginal increase from 10 kyr to 6 kyr (Fig. 5.22, Table 5.8).

Table: 5.8: ϵ_{Nd} and Nd concentration in the core 4032 and 4040.

Core: 4032

Depth (cm)	Age (years)	ϵ_{Nd}	Nd (ppm)
16-17	11646	-9.97	16.9
25-26	14876	-9.84	18.6
31-32	15654	-9.32	19.3
42-43	17080	-9.67	19.4
55-56	19292	-8.93	17.4
78-80	27809	-9.70	17.9
92-94	33173	-9.33	18.3
108-110	38574	-9.83	19.1

Core: 4040

Depth (cm)	Age (years)	ϵ_{Nd}	Nd (ppm)
4-5	5670	-11.01	13.7
11-12	9854	-11.17	13.8
14-15	11648	-9.68	15.1
21-22	15832	-9.21	18.1
26-27	18820	-8.11	18.9
32-34	22706	-8.51	21.1
44-46	29878	-9.07	19.9
48-50	32269	-10.48	15.7

Discussion

The G-B River system from the Himalayas, the Irrawaddy and Salween Rivers from the Indo-Burman ranges are the major contributors of terrigenous sediments to the Bay of Bengal. Studies have shown that sedimentation in the Bay of Bengal was modulated by glacio-eustatic sea level fluctuations, climate change and tectonic activity (Flood et al., 1995). Considering that the tectonic activity may be responsible for the long-term changes ($>10^5$ years) in sediment flux of riverine sediment (Schumm and Rea, 1995), climate change is largely responsible for variation in the sedimentation rate (Mulder and Syvitski, 1996). In view of this, the variation in sediment flux in the Bay of Bengal and the Andaman Sea can be used to reconstruct not only

the changing intensity of erosion and weathering in Himalayan and Burman regions (France–Lanord et al., 1993), but also towards reconstructing the past climatic conditions (Colin et al., 1999; Burton and Vance, 2000; Ahmed et al., 2005, 2008). For example, Colin et al. (1999) observed that between the Last Glacial Maximum (LGM) and Holocene a shift in the sea surface circulation pattern was invoked for the variation in detrital flux of G–B River system and western zone of Indo–Burman ranges (Colin et al., 1999). On a shorter time scale, variations in erosional patterns were directly related to the changes in monsoonal precipitation over the mountains. In recent studies, it has been demonstrated that sediment plumes originating from Irrawaddy River moves westwards during the northeast winter monsoon and eastwards during the southwest summer monsoon (e.g. Ramaswamy et al., 2004; Rao et al., 2005).

Sedimentation and Mass Accumulation Rates

In core 4032, it may be noted that there were significant variations in sedimentation rates during the last 50 kyr with a faster rate observed at ~ 20 kyr (Fig. 5.2). Similar observations have been made in the southeastern Arabian Sea indicating the post LGM enhanced sedimentation rates by a factor of 3–4 high compared to other periods during the past ~30 kyr (Agnihotri et al., 2001). The sedimentation rate at 4040 at the top of 90 East Ridge shows the least variation as it is located far off from the sediment source (Fig. 5.2).

In the central Bay of Bengal (core 4032), a discernable increase in sedimentation rate around 40 kyr was observed, this increase was also seen in the mass accumulation rate using major elements (Figs. 5.2 and 5.3). This period corresponds to the pluvial Marine Isotopic Stage–3 (MIS–3), with both marine and continental records indicating strengthened southwest monsoon conditions (Prell and Van Campo, 1986; Juyal et al., 2006). However, a prominent increase was observed in the mass accumulation rate after 20 kyr (post LGM) i.e. between 18 kyr and 14 kyr implying sediment mobilization that occurred during the transitional climatic condition following the LGM

(Goodbred Jr., 2003). The low sea level stand during the LGM led to the exposure of vast near coastal zone (Weber et al., 1997). As the climate began to ameliorate, these sediments were mobilized by increased runoff that probably outpaced the rising sea level. Weber et al. (1997) found sharp increase in terrigenous input around 15 kyr that continued till 12 kyr in the Bengal Fan which according to Goodbred Jr. (2003) is the first evidence for a post LGM revival of the Ganga dispersal system. After 14 kyr, the sea began to inundate a broad area of Bengal basin as the sea level rose to around 55 m below the present level by around 11 kyr. Consequently, majority of the sediment began to trap far inland causing a significant drop in the sedimentation rate on the upper Bengal Fan (Weber et al., 1997). This is indicated by significant decrease in sedimentation and mass accumulation rates after 14 kyr in the central Bay of Bengal (Fig. 5.3). However, compared to this, the southern Bay of Bengal (core 4040) shows a monotonous sedimentation rate except between 17 kyr and 15 kyr, when a marginal increase is observed. In the southern Bay of Bengal (core 4040), it is expected that major sedimentation variability would not be discernible due to its distal location from the influence of continental input and being on the top of the 90 East Ridge (Fig. 5.2).

Due to highly varying sedimentation rates in the Bay of Bengal, it is expected that the region experienced severe excursions in climate during the last ~50 kyr both due to sediment flux and overhead productivity. The Mass Accumulation Rates (MAR) calculated for the core 4032 reveals an interesting aspect of the changes in sedimentation and subsequently MAR (Fig. 5.3). The MAR in the Bay of Bengal was 3–5 $\text{g.cm}^{-2}.\text{kyr}^{-1}$ during 50 kyr till Last LGM. Around 17.5 kyr, a sudden enhanced MAR of $\sim 13 \text{ g.cm}^{-2}.\text{kyr}^{-1}$ was observed. This can only be explained by enhanced sedimentation post LGM bringing loads of sediments locked in the estuarine regions and from the exposed coastal zone (Agnihotri et al., 2003). Since, the sedimentation in the Bay of Bengal is controlled by the riverine input, enhanced monsoon conditions leads to large fresh water discharge. Thus, transitions from glacial–interglacial periods, wherein large sediment load is delivered to the

Bay due to enhanced freshwater flux, brings in sediments from the exposed coastal zones post LGM with low sea level.

Lithogenic Proxies

The detrital proxies measured in 4032 were also measured in core 4040, located in the southern Bay of Bengal. The down core variation of the concentration of the lithogenic proxies (Al, Fe, Mg and Ti) in both the cores shows decreasing trends after LGM (Figs. 5.4 and 5.5). Increased concentration in detrital proxies is expected due to the intensification of Southwest Summer monsoon (SWSM) during the post LGM. However, with the SWSM intensification, it is likely to have enhanced productivity that may cause a relative decrease in the concentrations of detrital proxies. Towards this, the location of core 4040, which is away from the direct influence of riverine fluxes, would respond to both changes in the detrital and overhead productivity (biogenic flux). With increasing distance from the coast, the sediment cores are expected to restore the productivity variations more efficiently than detrital variations. Sediment trap studies have showed that annual rain rates of particulate matter for lithogenic material decrease from north to south in the Bay of Bengal, and remained almost same for the carbonate and opal and high for C_{org} for northern and Central Bay of Bengal and slightly lower at the southern Bay of Bengal (Ramaswamy and Nair, 1994). This is clearly reflected in the Fe/Al, Mg/Al and Ti/Al ratios in core 4040 during the last ~36 kyr (Fig. 5.8). Although, these proxies do not show drastic changes, the variation suggests periodic changes in productivity as well as changes in the source of sediments during the glacial–interglacial transition. A general decrease in the ratios of detrital proxies since last the LGM to present is indicative of source variation with increasing productivity or intensification of the SW monsoon (Figs. 5.7 and 5.8). This decrease is due to an increase of biogenic component leading to a relative decrease in the detrital component (Al), finally resulting in an overall decrease of the ratios of detrital proxies. The last deglaciation was characterized by an increased

terrigenous input during 15700–14800 yr, and this is attributable to an early strengthening of summer monsoon activity in the region. Similarly, a remarkable increase in kaolinite content with reduced chlorite and illite was attributed to enhanced Holocene precipitation during 8800-6400 BP (Thamban et al., 2002).

Major elemental variation in the central Bay of Bengal shows a consistent increase between 50 kyr and 14 kyr. The reason being the period between 50 kyr and 30 kyr is considered as pluvial MIS-3 when the southwest monsoon was enhanced. Hence, it is expected that during this period (barring the short term instability) an overall increase in these elements should have been observed. This would imply that after MIS-3, sediment flux was influenced probably by the stronger northeast winter monsoon. There are evidences to suggest that the Bay of Bengal experienced enhanced winter monsoon (Sarkar et al., 1990; Tiwari et al., 2006). After 14 kyr, decreasing trend in major elements could be interpreted as due to the deposition of continental flux at the continental margins and deltas because of rising sea level.

Compared to this, in the southern Bay of Bengal, a weakened monsoon condition can be inferred around 30 kyr, followed by a distinct enhancement till 22 kyr. Around LGM, an overall decrease in overhead productivity suggests decreasing strength of the southwest monsoon. The monsoon appears to improve and peak around 14 kyr and 9 kyr. Similar patterns are also observed in the lithogenic proxies.

A rather detailed picture of monsoon variability emerges from the C/N ratio. In the central Bay of Bengal, terrigenous input giving rise to increased C/N ratios (>10) was attributed to enhanced monsoon conditions at about 35.5 kyr, 27 kyr (latter part of MIS-3), 18 kyr, 17 kyr, 13 kyr (post LGM) and 7 kyr (early Holocene) (Fig. 5.9). In the southern Bay of Bengal (location less modulated by small variations in detrital discharge), two

prominent periods of enhanced detrital input viz. 20 kyr and 12 kyr. After 20 kyr, a stepwise improvement in the monsoon can be suggested by the gradual increase in carbonate concentration. The sharp increase in C_{org} and C/N ratios after 20 kyr and 12 kyr is indicative of sediment mobilization during the transitional climatic condition following the LGM (Goodbred Jr., 2003; Fig. 5.10).

Biogenic Proxies

Stable isotopic analyses of organic carbon ($\delta^{13}C$) data from the central Bay of Bengal (core 4032) indicate dominance of marine organic matter between 50 kyr and 20 kyr, which thus implies a limited continental organic contribution. This could be due to the burial of organic matter in deltaic sediments during periods of enhanced monsoon condition at least during the MIS-3. However, after LGM, it can be suggested that the central Bay of Bengal began to receive organic carbon from the G-B River system due to low sea stand after LGM and the beginning of Holocene. The $\delta^{15}N$ of the C_{org} is expected to show effects of denitrification in case of anoxicity of bottom waters in the sediments (Altabet et al., 1999; Sarkar et al., 2000). The $\delta^{15}N$ values, however, do not show any large scale variation indicative of denitrification process in the region and range from 4–6‰ (Fig. 5.11). However, a close correlation of $\delta^{15}N$ with productivity is noticed in the downcore variation of the core (Banakar et al., 2005). The increase in $\delta^{15}N$ of the C_{org} during the Holocene signifies a period of high productivity causing enhanced denitrification within the subsurface waters, which is also reflected in its variation (Thamban et al., 2001; Agnihotri et al., 2003a). The $\delta^{15}N$ during the same period indicates reduced denitrification followed by enhanced denitrification process (Ganeshram et al., 2002).

A more robust proxy for palaeoproductivity are the ratios of Ca/Al, Ba/Al and Sr/Al. In the present case, only Ba/Al shows some variability which appears to be consistent with the proxies discussed above (Babu et al., 2002; Winkler et al., 2005). For example, a high ratio between 50 kyr

and 35 kyr (MIS-3) accords well with the monsoon induced enhanced productivity in the central Bay of Bengal (Fig. 5.12). Following this, a consistent low value till 18 kyr suggests a weakened productivity phase, after 15 kyr a stepwise increase in productivity implies gradual strengthening of the monsoon as observed in the carbonate variation. In the southern Bay of Bengal, though data are scanty below 30 kyr, based on the trends noticed it can be speculated that prior to 30 kyr (MIS-3), the region experienced enhanced productivity and after 30 kyr and prior to 20 kyr, a decrease in monsoon can be suggested (Agnihotri et al., 2003a). However, interestingly Ca/Al and Sr/Al shows an increase in productivity around 20 kyr (LGM), and this can be attributed to the enhanced northeast wind driven productivity in the southern Bay of Bengal. After 20 kyr, Ba/Al suggests a stepwise strengthening of the productivity implying a re-establishment of the southwest monsoon. Here, it is worth mentioning that a discernable low value around 8.5 kyr in all the three proxies indicates temporary weakening of the monsoon. Given the dating uncertainty, this could as well correspond to a short lived 8.2 kyr cooling event observed in the northern latitudes (Alley et al., 1993, 1997).

The Bay of Bengal is a region known for its rather high sedimentary input compared to any other oceanic region of the world due to several rivers draining into it which bring in a tremendous sediment load. During LGM, studies have shown that sediment input was reduced due to the locking of sediments in the continental margins and in the upper reaches of Himalaya (Goodbréd Jr., 2003). It was after the LGM, major flux of continental input was observed as indicated by the enhancement of lithogenic fluxes (Fig. 5.6). During such transitional periods increased organic carbon burial efficiency has been observed by (Galy and France-Lanord 2006; Galy et al., 2008). This is amply demonstrated by increase in fluxes of the redox sensitive elements viz. Mn, V and Cr after 20 kyr and 14 kyr in the central Bay of Bengal (Fig. 5.14). Near identical patterns with variability has also been observed in the

ratios of the above elements in the southern Bay of Bengal (Figs. 5.16 and 5.17).

Provenance Variation using Strontium and Neodymium Isotopes

Strontium in the Bay of Bengal sediments is deposited in both carbonate and silicate phases. In the carbonate phase, Sr is either associated with the carbonaceous overhead surface productivity or with the detrital carbonate component brought along with the rivers. While in the silicate fraction, strontium is mainly associated with detrital clay. The sediment with high radiogenic Sr to the Bay of Bengal is mainly contributed by the Himalayan Rivers compared to the other rivers draining the peninsular India and the Indo–Burman region. (Palmer and Edmond, 1989, 1992; Edmond, 1992; Krishnaswami et al., 1992 France–Lanord et al., 1993). On the contrary, the ϵ_{Nd} values of the sediments supplied by the peninsular rivers are either comparable or enriched compared to the Himalayan Rivers with low $^{87}Sr/^{86}Sr$. Hence, isotopic variation in the sediments of the Bay of Bengal can be inferred in terms of changes in the source of sediments and their transport pathways (Colin et al., 1999; Walter et al., 2000).

Colin et al. (1999) identified three end members responsible for the sedimentary distribution of $^{87}Sr/^{86}Sr$ in the Bay of Bengal. They are the Ganga River ($^{87}Sr/^{86}Sr \approx 0.735$ and $\epsilon_{Nd} \approx -15$), Irrawaddy River (≈ 0.713 , ≈ -11) and the Arakan coast (≈ 0.716 , -7.0). To ascertain the end member values of $^{87}Sr/^{86}Sr$ and ϵ_{Nd} of different possible sources for the sediments of the Bay of Bengal, Sr and Nd isotopic analyses was carried out for the bed sediments of the Ganga, Mahanadi, Godavari and Krishna at the river mouth. The Sr and Nd isotopic composition of river bed sediments of Ganga shows $^{87}Sr/^{86}Sr$ value of 0.76 and ϵ_{Nd} of -16 , for the Mahanadi river the values are 0.755 and -17 , for the Godavari river it is 0.72 and -14 and for the Krishna river the values are 0.72 and -12 .

Dispersion of sediment in the Bay of Bengal is influenced by the strengthening or weakening of the Southwest Summer Monsoon (SWSM) and Northeast Winter Monsoon (NEWM). During the winter monsoon, East India Coastal Current (EICC) flow moves southeastwards (during October to January period) whereas during the summer monsoon, the EICC flow direction changes to northeastward (February to September) (Tomczack and Godfrey, 1994).

The northern and the western Bay of Bengal receive sediments predominantly from G-B River system with minor contribution from the Irrawaddy River, which drains into the Andaman Sea. The Southwest monsoon is a major source of water for the G-B River system which has a larger catchment area. In comparison, the Irrawaddy river catchment is very small and the discharge is dependent on the winter monsoon precipitation. The high $^{87}\text{Sr}/^{86}\text{Sr}$ ratio (0.718–0.719) in these sediments is attributed to the Himalayan source sediments. The Irrawaddy river drains into the Andaman Basin and during the winter months the sediment input to the Bay of Bengal is prominent as the EICC moves southeastward. Recent studies has demonstrated that sediment plumes originating from Irrawaddy river moves westwards during the Northeast Winter Monsoon and eastwards during the Southwest Summer Monsoon (e.g. Ramaswamy et al., 2004; Rao et al., 2005). Therefore, together with the circulation pattern and low $^{87}\text{Sr}/^{86}\text{Sr}$ ratio around 43 kyr, 28 kyr, 20 kyr, 14 kyr and 6 kyr (Fig. 5.20) indicates a significant contribution from the Irrawaddy river system through the Arakan coast during weakened southwest monsoon. The higher $^{87}\text{Sr}/^{86}\text{Sr}$ ratio during the intervening periods is attributed to the high discharge and increased sediment flux from the Himalaya region during enhanced southwest monsoon (Fig. 5.20). Alternatively, the $^{87}\text{Sr}/^{86}\text{Sr}$ ratio can also be altered if the sediment provenance within Himalayan range changes from the Higher Himalayan Crystalline (HHC) which have low $^{87}\text{Sr}/^{86}\text{Sr}$ values compared to the Lesser Himalayan Crystalline (LHC) rocks (Jacobsen et al., 2002; Singh et al., 2008). Studies on glaciations patterns in the Himalayas suggest that during periods

of weak southwest monsoon, Higher Himalaya regions were snow covered (Owen et al., 2005). In view of this, it is reasonable to assume that sediment supply from the HHC with low $^{87}\text{Sr}/^{86}\text{Sr}$ ratio would have been reduced and the dominant sediments supply was from the LHC with a high $^{87}\text{Sr}/^{86}\text{Sr}$ ratio. The above scenario seems to be less likely for the simple reason that in such situations high $^{87}\text{Sr}/^{86}\text{Sr}$ ratio should have been preserved around 20 kyr (LGM), which has not been observed here. The other possible source of material with low $^{87}\text{Sr}/^{86}\text{Sr}$ ratio could have been from the peninsular rivers ($^{87}\text{Sr}/^{86}\text{Sr}$ ratio ~ 0.715 - 0.725) (Ahmad et al., 2005). In the present study (Chapter-4), it has been demonstrated that $^{87}\text{Sr}/^{86}\text{Sr}$ ratio of surface sediment in the Bay of Bengal near the eastern coast of India range from 0.715 to 0.720 suggesting significant influence by G-B River system, almost masking the affect of peninsular rivers even in the near coastal regions.

The low $^{87}\text{Sr}/^{86}\text{Sr}$ represent periods of weakened SWSM at the expense of strengthened NEWM leading to enhanced supply of low radiogenic $^{87}\text{Sr}/^{86}\text{Sr}$ from the Irrawaddy River along the Arakan coast through the southeastward movement of EICC. In order

to attest to this hypothesis, Nd isotopic composition

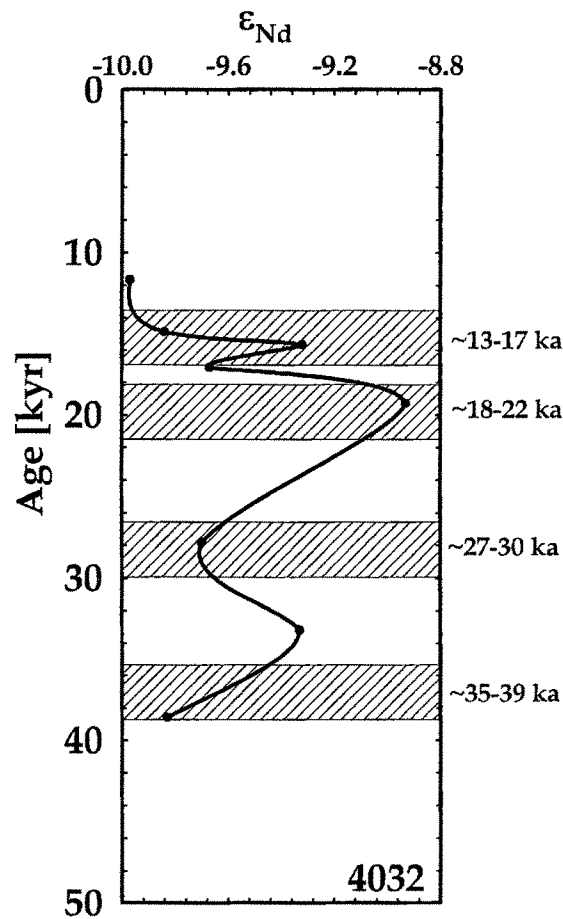


Fig 5.21 Downcore variation of ϵ_{Nd} in the silicate fraction of the sediments from the core 4032. Note, the lowest ϵ_{Nd} of -8.8 at 20 kyr

(ϵ_{Nd}) in the silicate fraction of select sediment samples from the two cores were analysed. The ϵ_{Nd} in the core 4032 varies from -10 to -8.9 and in core 4040 from -11 to -8. The high ϵ_{Nd} values in core 4032 at 20 kyr are -8.9 and -9.4 corresponding to 16 kyr and 34 kyr, respectively (Fig. 5.21). In core 4040, however, the only high of ϵ_{Nd} of -8.0 corresponds to 20 kyr (Fig. 5.22). Such high values of ϵ_{Nd} have not been observed in the sediments of the other major rivers draining into the Bay of Bengal (Galy and France-Lanord, 2001; Colin et al., 1999). However, the highest ϵ_{Nd} measured in the Irrawaddy river is at the river's mouth in the Andaman Sea where the value is -11 and there is no data available for ϵ_{Nd} in the suspended sediments of the Irrawaddy river. It is thus probable that the western fan of the Irrawaddy river is a likely candidate for the high radiogenic ϵ_{Nd} to the Bay of Bengal. Singh and France-Lanord (2002) observed very high values of ϵ_{Nd} (-6.9 and -8.4) in the sediments of the eastern tributaries of Brahmaputra (Dibang and Dhansiri) draining through the Trans Himalayan plutonic belt and Indo-Burman ranges. A similar lithology is found in the Irrawaddy river basin. Considering the above, it is speculated at this stage (due to lack of suspended load data) that the Irrawaddy river is probably the source of more radiogenic ϵ_{Nd} into the Bay of Bengal. Based on the above premise, it is suggested that during

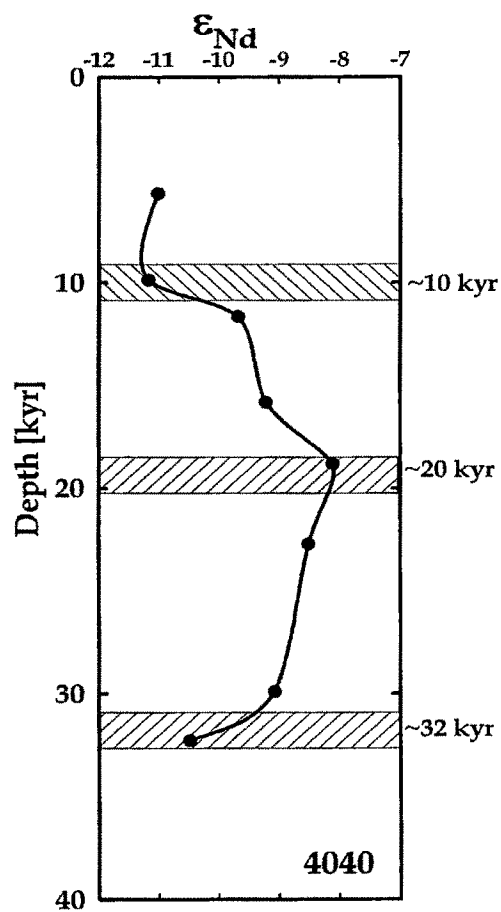


Fig.5.22 Downcore variation of ϵ_{Nd} in the silicate fraction of the sediments from the core 4040. Note, the lowest ϵ_{Nd} of -8.0 at 20 kyr

LGM, strengthened NEWM high sediment flux from the Arakan coast was routed through the Irrawaddy river to the eastern Bay of Bengal.

Together with the Sr and the Nd isotopic variations as seen in the two sediment cores, it can be inferred that during LGM the SWSM was weaker with a correspondingly strengthened NEWM. Based on other geochemical proxies and Nd isotopic variation, amelioration of the NEWM can be suggested from 32 kyr to 20 kyr. However, from 20 kyr (LGM) to 10 kyr, amelioration of the SWSM is clearly discernible.

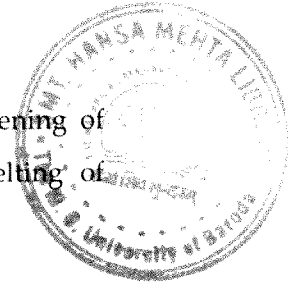
Regional and Global Correlations

The physical, biological and chemical environment of the Bay of Bengal is closely linked to the variation in the summer and winter monsoon systems of the Indian subcontinent (Shetye et al., 1993). The monsoonal system of the Indian Ocean as a whole is one of the major atmospheric components of the tropical climate patterns where there are large seasonal variations with intensive rainfall during summer. During the northern winter, dry cold winds from the Asian continent flows off shore (McGregor and Nieuwolt, 1998). The monsoonal cycle dominates the fluvial runoff of one of the world's largest rivers systems viz. the Ganga and Brahmaputra system, which drains most of the Himalayas and the northern Indian subcontinent. Himalayan rivers are typically characterized by very high topography particularly on the southern Himalayan flank (boundary between the Lesser and Higher Himalaya). This front receives the major blast of the southwest monsoon resulting in intense physical erosion of the area (Seeber and Gortniz, 1983). Within the Himalayan basin, modern accumulation of eroded material represents a very minor reservoir compared to the Bay of Bengal (Bengal fan). In view of this, changes in sedimentation rate, geochemistry and isotopic proxies used in the present study enable us to reconstruct the variation in monsoon intensity during the last 50 kyr (Henderson, 2002). Three major climatic excursions as recorded in the sediment cores suggests enhanced monsoon during MIS-3 (between 50 kyr and 30 kyr), a weakening of the monsoon around LGM

(dated to 20 kyr) and a post glacial strengthening of the monsoon (after 20 kyr and 10 kyr). Within these periods, low frequency and low amplitude fluctuations have been recorded. It is observed that around 14 kyr, all proxies indicate enhanced summer monsoon conditions. Continental record from India, though limited, corroborates well with these observations. For example, during the MIS-3 valley glaciers receded in Central Himalaya suggest improved monsoonal condition. In the Central Ganga plain, Thar desert, western and Central India, regional flood plain aggradation and pedogenesis during the MIS-3 (50 kyr and 30 kyr) are attributed to an enhanced phase of monsoon activity (Kale and Rajaguru, 1987; Andrews et al., 1998, Singh et al., 1999; Srivastava et al., 2001; Jain and Tandon, 2003; Juyal et al., 2006). Considering the duration (<60 kyr and 30 kyr) and regional nature of this event, it was suggested that southwest monsoon was probably similar to or wetter than today (Juyal et al., 2006).

Gradual initiation of the weakening of monsoon is interpreted based on the decrease in mass accumulation rate, and productivity that began after 30 kyr and continued till around 20 kyr (LGM). In Himalaya, less extensive valley glaciation during this period was attributed to the weakening of the southwest monsoon (Benn and Owen, 1998; Pant et al., 2006). The Lesser Central Himalayan lake sediments suggest an arid phase between 25.6 kyr and 21.5 kyr (Kotlia et al., 1997; 2000). In the southern margin of the Thar desert, evidence suggests that the summer monsoon began to dwindle after 30 kyr and peak aridity appeared around 20 kyr (Juyal et al., 2003 and 2006). After 20 kyr, an abrupt increase in mass accumulation rate (after 20 kyr and 14 kyr) suggests mobilization of the sediments in the Himalaya region after the recession of valley glaciers (Goodbred Jr., 2003). In the Higher Central Himalaya after 20 kyr, deposition of sand in otherwise varve dominated lakes was attributed to post LGM warming (Juyal et al., 2004). Sinha et al. (2005) based on oxygen isotopic variation in a stalagmite collected from Timta cave in western Himalaya show multi-decadal monsoon variability between 15.2 kyr and 11.7 kyr. According to them, a progressive depletion in oxygen

isotope value between 15.2 kyr to 14.3 kyr is due to the strengthening of monsoon intensity and the addition of ^{16}O to the ocean by melting of Himalayan ice sheets.



In the Bay of Bengal and the Andaman Sea cores, study based on the magnetic grain size and CIA variations show prominent cooling events (weak monsoon) around 21 kyr and 14 kyr punctuated by a marginal improvement in monsoon (Colin et al., 1998). This is further corroborated by Kudrass et al. (2001) suggesting enriched oxygen isotope value and relatively high salinity around 21 kyr and 14 kyr which they attributed to the reduced hydrological discharge from Himalayan regions. Similarly, in the Arabian Sea sediments the percentage change in *G. Bulloides* around 14.5 kyr is attributed to an abrupt increase in monsoon strength (Overpeck et al., 1996). Based on the organic carbon variation, in the northeastern Arabian Sea, Schulz et al. (1998) have suggested weak monsoon periods around 23 kyr and 15 kyr, whereas the intervening period (between 23 kyr and 15 kyr) were identified as strengthened monsoon conditions. Based on the above, it can be suggested that multi-millennial climatic variability accords reasonably well with the continental and marine records obtained in earlier study. This would imply that climate variability reconstructed from the Bay of Bengal core responded to a regional climatic system.

In core 4032, only two distinct events of low productivity are noticed at 12 kyr and 14.6 kyr coinciding with H0 and H1 respectively. H0 event was also seen in 4040 but was bit dampened in 4032 (Fig. 5.12). But H0 and H1 events are clearly discernible in the Bay of Bengal with decreased productivity thereby indicating its strength and its effect in low latitudes. Most of other high or low productivity events seem to have been masked in 4032 by the high detrital component at this location. Additionally, both the cores, in all their biogenic proxies show continuous increase from LGM to present reflecting intensification of SW monsoon during the last 20 kyr. The periods of strengthened monsoon conditions can be noticed from events such as high

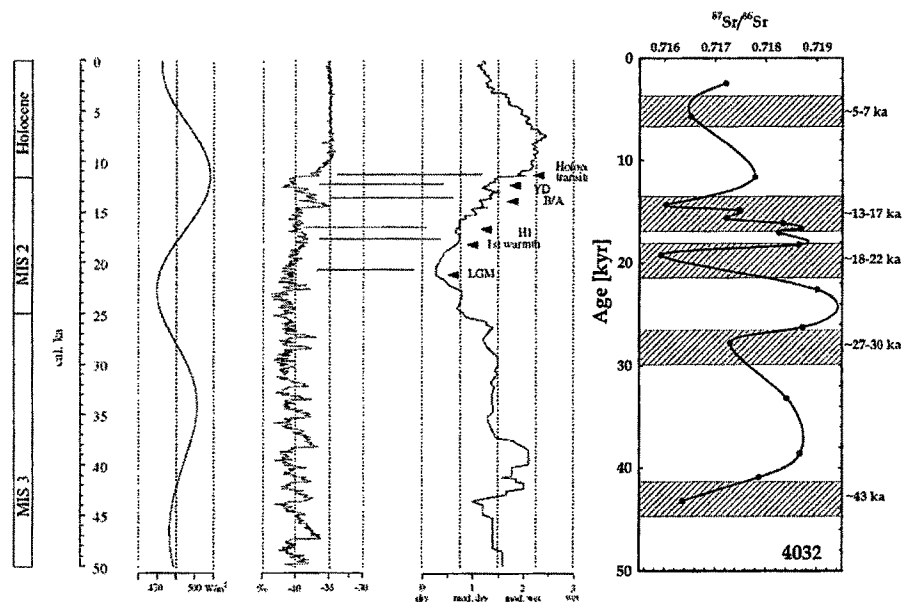


Fig. 5.23: Comparison of $^{87}\text{Sr}/^{86}\text{Sr}$ with solar insolation and mean effective moisture (Herzschuh et al., 2006). Note, synchronous variation of $^{87}\text{Sr}/^{86}\text{Sr}$ with solar insolation and moisture indicative of global correlation of the Bay of Bengal climate.

productivity. There are evidences for rapid changes in climate during LGM in tropical Atlantic (Hughen et al., 1996).

An important observation made during the present study is the implication of $^{87}\text{Sr}/^{86}\text{Sr}$ ratio and ϵ_{Nd} towards reconstructing the summer and winter monsoon variability provided the cores are strategically selected. It has been demonstrated that periods of winter rainfall are associated with low $^{87}\text{Sr}/^{86}\text{Sr}$ ratio and high ϵ_{Nd} and vice versa (Fig. 5.23). Synchronous variation in solar insolation, mean effective moisture and $^{87}\text{Sr}/^{86}\text{Sr}$ in the core 4032 is observed. The dry period corresponds to low $^{87}\text{Sr}/^{86}\text{Sr}$ is indicative of low detrital discharge from the G-B River system, which coincides with low solar insolation (Herzschuh, 2006).

Continental and marine records discussed above show near synchronous changes in monsoon variability during the last 50 kyr. Such changes have been attributed to coupled global and local processes (Gasse

and Van Campo, 1994; Prell and Kutzbach, 1987, 1992). For example, coherency between low-latitude monsoonal climate variability and rapid temperature fluctuations as observed in the Greenland ice record during the last glacial stage provides a link to climate in geographically distinct parts of the world (Schulz, et al., 1998; Rashid et al., 2007). Schulz et al. (1998) have demonstrated that during the north Atlantic interstadials, monsoon induced biological productivity was high in the northeastern Arabian sea whereas periods of low productivity was associated with high latitude atmospheric cooling and the injection of melt water into the North Atlantic basin. Zonneveld et al. (1997) suggested that the connectivity between the North Atlantic climate and summer monsoon is likely to be atmospheric. According to Colin et al. (1998), any changes in the boundary conditions of high latitudes should modify the amount and timing of cold air transported towards the south, which in turn influences the formation and development of the low surface pressure above the Tibetan Plateau. A westerlies–swinging model was proposed by Fang et al. (1999) to demonstrate the climatic connectivity between northern latitude and Asian monsoon variability. According to their model, during high-insolation periods (interglacials/interstadials) strong low pressure develops over Tibet (Tibetan low), as a result of which westerlies stay north of the Tibetan Plateau causing enhancement of the summer monsoon through northward propagation of moisture laden winds and the converse happens during the low-insolation periods. Recent studies have shown that during the intensified monsoon phases in the late Pleistocene and Holocene time, moisture migrated into the high arid part of the northwest Himalaya which in turn enhanced the sediment flux compared to the present day weaker monsoon condition (Bookhagen et al., 2005b).

Climatic Periodicities from Proxies

The solar radiation reaching the earth surface has been varying with time and shows periodicity in its variation with the solar insolation cycles. These variations in the total solar irradiance result in global changes in the climate (Milankovich, 1920; Imbrie, 1985; Haigh, 2001). While solar irradiance

supplies the periodic forcing, the coupled ENSO–monsoon anomalies provide the amplification for these signals to appear in climate archives (Higginson et al., 2004). The Earth’s climate system is highly sensitive to extremely weak perturbations in the Sun’s energy output on the centennial to millennial time scales. The apparent solar response was robust in the North Atlantic even as early Holocene (Bond et al. 2001). These changes in the climate are stored in proxies stored in various repositories. The marine sediments are one such repository which preserves these signatures. The short term climatic oscillations are obliterated in the marine records due to bioturbation of the sediments by the burrowing animals. Additionally, it becomes difficult to retrieve short-term fluctuations as the deep-sea sediments are deposited at slower rates of 1–10 cm/kyr.

In this study, from the undisturbed record of detrital and biogenic proxies from two cores in the Bay

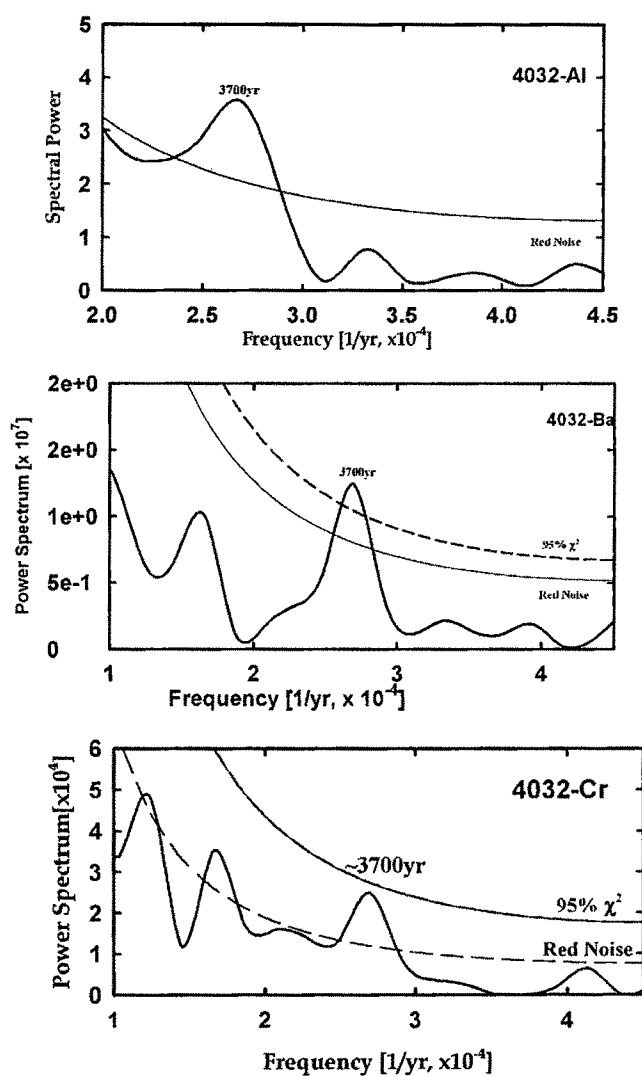


Fig. 5.24: Periodicities observed in the core 4032 in various proxies. Note 3.7 kyr periodicity prominent in all the proxies.

of Bengal (4032 and 4040), some of these millennial scale periodicities of climatic oscillations are derived by Fourier analyses of these data. Leuschner and Sirocko (2003) based on high-resolution record of upwelling and dust flux from the western Arabian Sea found resemblance to an insolation-based Indian Summer Monsoon Index. The insolation forcing in the low latitudes directly controls atmospheric processes in the African, Indian and Asian Monsoon, responsible for huge amount of trans-equatorial water vapour and therefore latent heat transport. The millennial-scale variability of the monsoonal

climate is noticed at periodicities near 100, 1450, 1750 and 2300 yrs (Agnihotri et al., 2002; Leuschner and Sirocko, 2003).

To ascertain the forcing factors responsible for the cyclic fluctuations in the lithogenic and biogenic proxies in cores 4032 and 4040, spectral analysis was performed

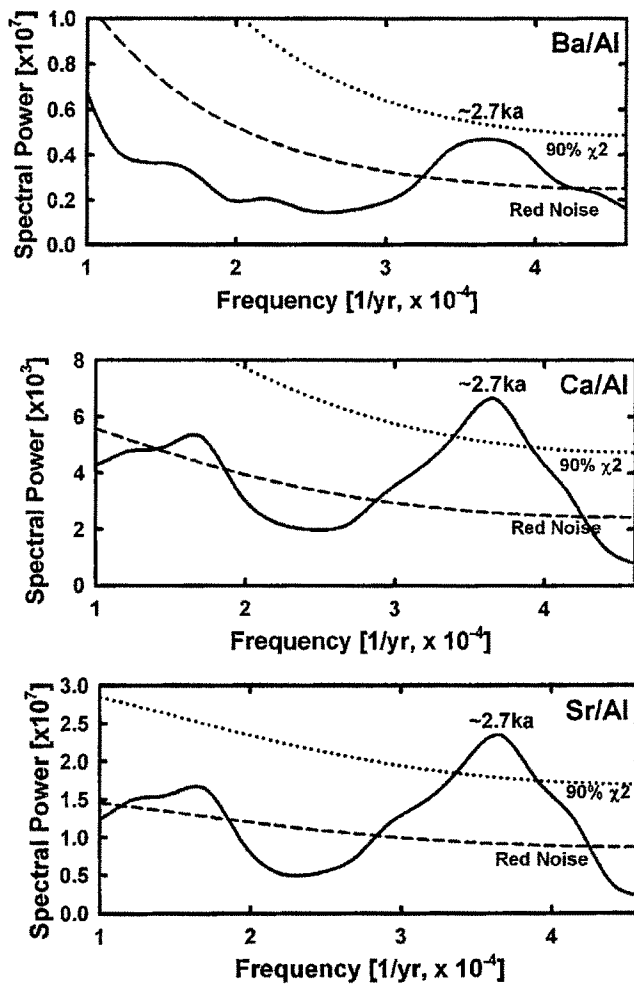


Fig. 5.25: Periodicities observed in the core 4040 in productivity proxies. Note 2.7 kyr periodicity prominent in all the proxies.

using the standard methods (Schulz and Stattegger, 1997; Schultz et al., 1998; Schulz and Mudelsee, 2000) applicable for geochemical data for unevenly spaced time series data (Figs 5.24, 5.25, 5.26). This method determines a theoretical red noise level and a false alarm level based on first order autoregressive (AR1) process algorithm. False alarm level is the maximum spectral amplitude expected if the time series would have been generated by AR1 process. Spectral peaks with amplitudes less than the theoretical red

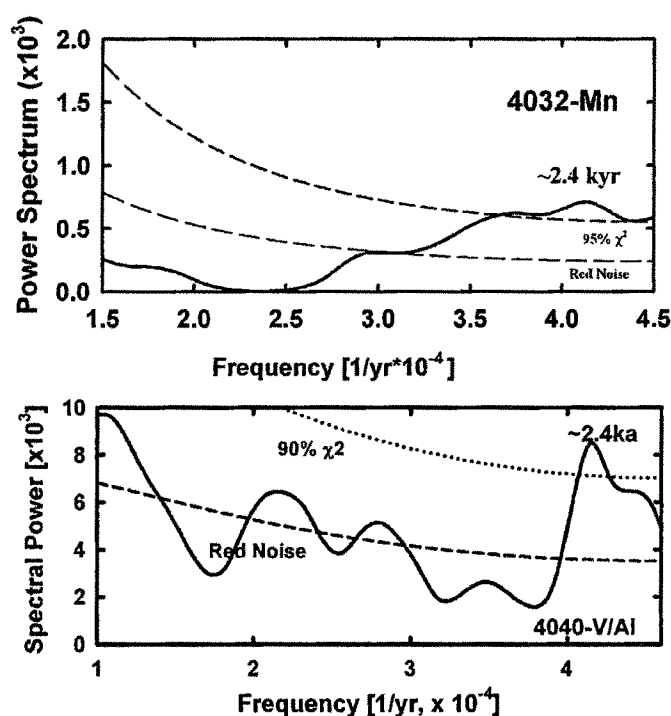


Fig. 5.26.: Periodicities observed in the core 4032 for Mn and V/Al. Note 2.4 kyr periodicity prominent in all the proxies.

noise level are rejected and exceeding or close to the false alarm level (above 80 to 95% confidence level) indicate non-AR1 component and are considered "significant".

The spectral analysis of the detrital, productivity and redox sensitive proxies were carried out in both the cores 4032 and 4040 (Fig. 5.24, 5.25 and Fig. 5.26). Three dominant periodicities of 2.4, 2.7 and 3.7 kyr are noticed in various proxies in both the cores. The 2.5, 2.77 and 3.95 kyr periodicities have

been confirmed to be of solar origin of insolation cycles from speleothem records (Stoykova et al., 2008). The synchronous retrieval of various periodicities indicates solar forcing of climate and its variations in the Bay of Bengal with these cycles. High resolution records can provide much more conclusive evidence for these periodicities. The solar influence on monsoon activity is not due to a change in radiative heating in the troposphere, rather, originates from the stratosphere through modulation of the upwelling in the equatorial troposphere, which produces a north-south seesaw of convective activity over the Indian Ocean sector, during summer. High precipitation over Arabia and India, thus, occurs during high solar activity (Kodera 2004).